

PB85 162297



U.S. Department
of Transportation
**Federal Railroad
Administration**

Fatigue Crack Initiation Properties of Rail Steels

Office of Research
and Development
Washington, DC 20590

R. C. Rice
D. Broek

Battelle Columbus Laboratories
505 King Avenue
Columbus, Ohio 43201

DOT/FRA/ORD-82/05

March 1982
Final Report

This document is available to the
U.S. public through the National
Technical Information Service,
Springfield, Virginia 22161.

Office of the Secretary of Transportation
Washington, D.C. 20590

NOTICE

This document is disseminated under the sponsorship of the Department of Transportation in the interest of information exchange. The United States Government assumes no liability for its contents or use thereof.

NOTICE

The United States Government does not endorse products or manufacturers. Trade or manufacturers' names appear herein solely because they are considered essential to the object of this report.

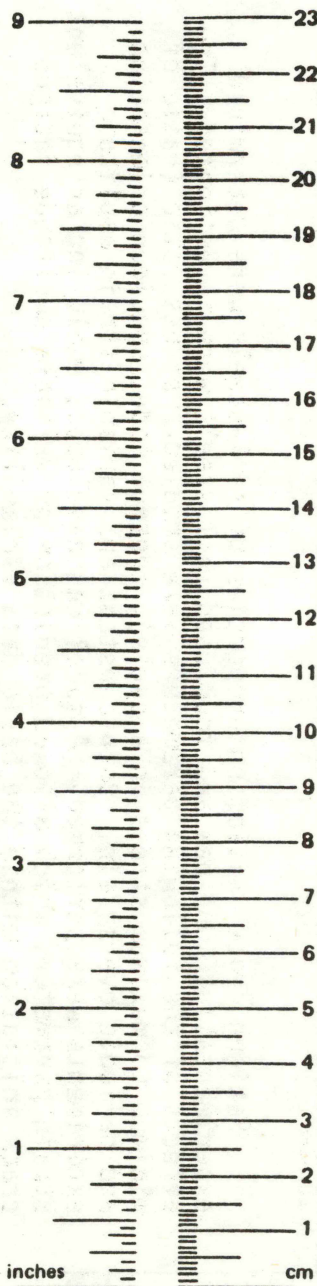
1. Report No. FRA/ORD-82-05		2. Government Accession No.		3. Recipient's Catalog No.	
4. Title and Subtitle FATIGUE CRACK INITIATION PROPERTIES OF RAIL STEELS			5. Report Date March 1982		
			6. Performing Organization Code		
7. Author(s) R. C. Rice, D. Broek			8. Performing Organization Report No. DOT-TSC-FRA-81-22		
9. Performing Organization Name and Address Battelle Columbus Laboratories* 505 King Avenue Columbus, OH 43201			10. Work Unit No. (TRAIS) RR119/2309		
			11. Contract or Grant No. DOT-TSC-1426		
12. Sponsoring Agency Name and Address U.S. Department of Transportation Federal Railroad Administration Office of Research and Development Washington, D.C. 20590			13. Type of Report and Period Covered Final Report		
			14. Sponsoring Agency Code		
15. Supplementary Notes *Under contract to: U.S. Department of Transportation Research and Special Programs Administration Transportation Systems Center Cambridge, MA 02142					
16. Abstract Fatigue crack initiation properties of rail-steels were determined experimentally. One new and four used rail steels were investigated. The effects of the following parameters were studied: stress ratio (ratio of minimum to maximum stress in a cycle), control mode, specimen orientation, and periodic overstrain. Both constant and variable strain amplitude experiments were performed. A model was developed, employing an equivalent strain parameter, which allowed prediction of variable amplitude fatigue crack initiation within the basic data variability.					
17. Key Words Rail, Crack Initiation, Fatigue, Periodic Overstrain, Equivalent Strain.			18. Distribution Statement Document is available to the public through the National Technical Information Service, Springfield, Virginia 22161		
19. Security Classif. (of this report) Unclassified		20. Security Classif. (of this page) Unclassified		21. No. of Pages 68	22. Price

METRIC CONVERSION FACTORS

Approximate Conversions to Metric Measures

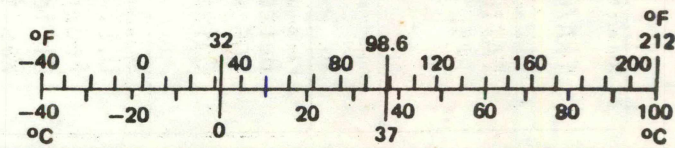
Symbol	When You Know	Multiply by	To Find	Symbol
LENGTH				
in	inches	*2.5	centimeters	cm
ft	feet	30	centimeters	cm
yd	yards	0.9	meters	m
mi	miles	1.6	kilometers	km
AREA				
in ²	square inches	6.5	square centimeters	cm ²
ft ²	square feet	0.09	square meters	m ²
yd ²	square yards	0.8	square meters	m ²
mi ²	square miles	2.6	square kilometers	km ²
	acres	0.4	hectares	ha
MASS (weight)				
oz	ounces	28	grams	g
lb	pounds	0.45	kilograms	kg
	short tons (2000 lb)	0.9	tonnes	t
VOLUME				
tsp	teaspoons	5	milliliters	ml
Tbsp	tablespoons	15	milliliters	ml
fl oz	fluid ounces	30	milliliters	ml
c	cups	0.24	liters	l
pt	pints	0.47	liters	l
qt	quarts	0.95	liters	l
gal	gallons	3.8	liters	l
ft ³	cubic feet	0.03	cubic meters	m ³
yd ³	cubic yards	0.76	cubic meters	m ³
TEMPERATURE (exact)				
°F	Fahrenheit temperature	5/9 (after subtracting 32)	Celsius temperature	°C

*1 in. = 2.54 cm (exactly). For other exact conversions and more detail tables see NBS Misc. Publ. 286, Units of Weight and Measure. Price \$2.25 SD Catalog No. C13 10 286.



Approximate Conversions from Metric Measures

Symbol	When You Know	Multiply by	To Find	Symbol
LENGTH				
mm	millimeters	0.04	inches	in
cm	centimeters	0.4	inches	in
m	meters	3.3	feet	ft
m	meters	1.1	yards	yd
km	kilometers	0.6	miles	mi
AREA				
cm ²	square centimeters	0.16	square inches	in ²
m ²	square meters	1.2	square yards	yd ²
km ²	square kilometers	0.4	square miles	mi ²
ha	hectares (10,000 m ²)	2.5	acres	
MASS (weight)				
g	grams	0.035	ounces	oz
kg	kilograms	2.2	pounds	lb
t	tonnes (1000 kg)	1.1	short tons	
VOLUME				
ml	milliliters	0.03	fluid ounces	fl oz
l	liters	2.1	pints	pt
l	liters	1.06	quarts	qt
l	liters	0.26	gallons	gal
m ³	cubic meters	36	cubic feet	ft ³
m ³	cubic meters	1.3	cubic yards	yd ³
TEMPERATURE (exact)				
°C	Celsius temperature	9/5 (then add 32)	Fahrenheit temperature	°F



PREFACE

This report presents the results of a program on rail steel fatigue crack initiation characterization. It has been prepared by Battelle's Columbus Laboratories (BCL) under Task 3 of Contract DOT-TSC-1426 for the Transportation Systems Center (TSC) of the Department of Transportation. Work was begun under the technical direction of Roger Steele of TSC and subsequently completed under the supervision of Oscar Orringer of TSC.

The experimental work was performed in the Fatigue Laboratory of Battelle's Columbus Laboratories by Norman Frey, whose care and concern are gratefully acknowledged. The development of nondestructive crack initiation monitoring techniques was handled by Ms. Karen Pfister. Her efforts are also appreciated. Some assistance on data analysis was also gratefully received from Ronald Galliher.

TABLE OF CONTENTS

<u>Section</u>		<u>Page</u>
	EXECUTIVE SUMMARY.....	1
1	INTRODUCTION.....	3
2	RAIL MATERIALS.....	4
3	EXPERIMENTAL DETAILS.....	5
	3.1 Specimens.....	5
	3.2 Testing Procedures.....	5
	3.3 Crack Initiation Detection.....	10
4	TEST RESULTS.....	13
	4.1 Constant Amplitude Experiments.....	13
	4.1.1 Unused Rail Data.....	13
	4.1.2 Used Rail Data.....	18
	4.2 Periodic Overstrain Experiments.....	25
	4.3 Variable Strain Amplitude Experiments.....	29
5	DAMAGE ACCUMULATION MODEL.....	36
	5.1 Definition of Initiation Crack Size.....	36
	5.2 Statistical Definition of Constant Amplitude Fatigue Data.....	39
	5.2.1 Unused Rail Crack Initiation Data.....	39
	5.2.2 Used Rail Crack Initiation Data.....	45
	5.3 Variable Strain Amplitude Crack Initiation Prediction.....	45
	5.4 Implementation of Damage Model in a Reliability Analysis.....	56
6	CONCLUSIONS.....	57
7	REFERENCES.....	58

LIST OF ILLUSTRATIONS

<u>Figure</u>		<u>Page</u>
1	BCL UNIAXIAL FATIGUE TEST SPECIMEN.....	6
2	BCAC UNIAXIAL FATIGUE TEST SPECIMEN.....	6
3	TRANSVERSE RAIL UNIAXIAL FATIGUE TEST SPECIMEN.....	7
4	CENTER-HEAD SPECIMEN LOCATION	7
5	INTERMEDIATE SPECIMEN LOCATION.....	8
6	SURFACE SPECIMEN LOCATION.....	9
7	ULTRASONIC TRANSDUCER SETUP.....	11
8	HEAT-TINTED CRACK INITIATION ZONE ON SPECIMEN 2-11-E.....	11
9	RATIO OF INITIATION CYCLES TO TOTAL FAILURE CYCLES AS A FUNCTION OF CRACK DEPTH.....	14
10	MONOTONIC AND CYCLIC STRESS-STRAIN BEHAVIOR OF CENTER-HEAD RAIL SPECIMENS.....	14
11	MONOTONIC AND CYCLIC STRESS-STRAIN BEHAVIOR OF SURFACE-HEAD RAIL SPECIMENS.....	15
12	MONOTONIC AND CYCLIC STRESS-STRAIN BEHAVIOR ON TRANSVERSE-HEAD RAIL SPECIMENS.....	16
13	STRESS-STRAIN HYSTERESIS LOOPS FOR SPECIMEN 1-6-E THROUGH FIRST FIVE CYCLES AT 0.8-PERCENT STRAIN RANGE.....	17
14	FATIGUE LIFE VS. EQUIVALENT STRAIN FOR CENTER-HEAD RAIL SPECIMENS.....	24
15	FATIGUE LIFE VS. EQUIVALENT STRAIN FOR SURFACE-, INTERMEDIATE-, AND TRANSVERSE-HEAD RAIL SPECIMENS, $R = 1.0$	24
16	FATIGUE LIFE TRENDS FOR USED RAIL MATERIAL.....	27
17	PERIODIC OVERSTRAIN FATIGUE TEST RESULTS.....	27
18	CUMULATIVE PROBABILITY PLOT OF PEAK VERTICAL WHEEL RAIL LOADS.....	31
19	TRAIN COMPOSITIONS FOR TRAIN-BY-TRAIN AND RANDOM HISTORIES.....	33
20	PART OF THE STRAIN HISTORY OF THE 11-LOAD RANDOM SERVICE SIMULATION EXPERIMENTS.....	33
21	THRESHOLD VS. ENDURANCE LIMIT FOR $R = -1.0$	37
22	THRESHOLD VS. ENDURANCE LIMIT FOR $R = 0.10$	37
23	THRESHOLD VS. ENDURANCE LIMIT FOR $R = 0.50$	38
24	APPARENT OR EQUIVALENT INITIAL FLOW TRANSITION CRACK LENGTH (EIF) BETWEEN INITIATION AND PROPAGATION FOR RAIL STEEL FATIGUE SPECIMENS...	38
25	FATIGUE LIFE TRENDS FOR GROUPED DATA VS. EQUIVALENT STRAIN.....	40
26	LOG NORMAL PROBABILITY PLOT OF UNUSED RAIL CRACK INITIATION DATA.....	41
27	TWO-PARAMETER WEIBULL OF UNUSED RAIL CRACK INITIATION DATA.....	42
28	USED RAIL DATA, STRESS LEVELS COMBINED.....	47

LIST OF ILLUSTRATIONS (Continued)

<u>Figure</u>		<u>Page</u>
29	USED RAIL DATA, STRESS LEVELS PLOTTED SEPARATELY.....	48
30	METHOD 1, CONSTANT AMPLITUDE CURVE AND ACTUAL MAXIMUM STRESSES (UNIT TRAIN ONLY).....	54
31	METHOD 2, PERIODIC OVERSTRAIN WITH ACTUAL σ_{max}	54
32	METHOD 3, PERIODIC OVERSTRAIN WITH CALCULATED σ_{max}	55

LIST OF TABLES

<u>Table</u>		<u>Page</u>
1	USED RAIL MATERIAL BACKGROUND DATA.....	4
2	RAIL SPECIMEN INVENTORY.....	5
3	COMPLETE LISTING OF ALL BCL AND BCAC CONSTANT AMPLITUDE CRACK INITIATION TEST DATA ON UNUSED RAILS.....	19
4	SUMMARY OF USED RAIL FATIGUE TEST RESULTS.....	26
5	PERIODIC OVERSTRAIN TEST RESULTS ON NEW RAIL MATERIAL.....	28
6	COMPUTATION OF RELATIVE DAMAGE CAUSED BY LARGE AND SMALL CYCLES IN PERIODIC OVERSTRAIN.....	29
7	COMPARISON IN NUMBER OF NONDAMAGING SMALL CYCLES IN PERIODIC OVERLOAD EXPERIMENTS.....	30
8	VARIABLE STRAIN AMPLITUDE FATIGUE TEST RESULTS.....	34
9	STABLE STRESS RESPONSE OF UNIT TRAIN TEST SPECIMENS.....	35
10	GROUPED AND RANKED CRACK INITIATION DATA ON UNUSED RAIL MATERIAL.....	43
11	GROUPED AND RANKED CRACK INITIATION DATA ON USED RAIL MATERIAL.....	46
12	ONE-HALF FEC PLUS ONE-HALF UP UNIT TRAIN FATIGUE DAMAGE CALCULATIONS.....	49
13	NEC UNIT TRAIN FATIGUE DAMAGE CALCULATIONS.....	50
14	SP UNIT TRAIN FATIGUE DAMAGE CALCULATIONS.....	51
15	FATIGUE DAMAGE CALCULATIONS FOR RANDOM AND TRAIN-BY-TRAIN SPECTRA (METHOD 3).....	52
16	ESTIMATED AND ACTUAL SPECIMEN CYCLES TO FAILURE FOR VARIABLE AMPLITUDE TESTS.....	53

EXECUTIVE SUMMARY

This report presents part of the results of a study on rail material characterization for the correlation of rail defect growth and failure properties to better define rail defect mechanisms. The work was conducted as part of the Track Structures Research Program under the direction of the Transportation Systems Center and sponsored by the Federal Railroad Administration. The results are presented in two volumes entitled:

Determination of Residual Stresses in Rails

Fatigue Crack Initiation Properties of Rail Steels.

This report describes an experimental study in which the objective was to determine fatigue crack initiation properties of standard American Railway Engineering Association (AREA) rail steel. The fatigue life of structural components is determined by the sum of the loads and stress cycles required to initiate a fatigue crack and to propagate that crack from subcritical dimensions to a critical crack size. Thus, knowledge of fatigue crack initiation properties, which crack propagation models do not address, is necessary for a complete assessment of rail life.

One new and four used rail steels were investigated. The influence on crack initiation behavior of stress ratio, control mode, orientation within the rail and periodic overstrain were investigated. Both constant and variable amplitude experiments were performed. An analytical model was developed, employing an equivalent strain parameter, which allowed prediction of variable amplitude (service load) fatigue crack initiation from constant amplitude material characterization data.

From this study it can be concluded that periodic overstrains above the constant amplitude fatigue limit will substantially increase the damage caused by strain ranges below the limit, and a periodic overstrain fatigue curve should be used in life predictions on such spectra. Accordingly the entire range of traffic loads must be considered, not just isolated overloads. Transverse rail head cracks were found to initiate more rapidly than longitudinal rail head cracks, and the relative susceptibility of various head locations to rail fatigue failure was identified. Also, it was demonstrated that linear damage accumulation models can be used effectively to provide reasonable crack initiation life predictions.

1. INTRODUCTION

A typical failure in a rail is the culmination of a progressive damage process that begins with the initiation of a fatigue crack, followed by the growth of that crack to a critical size. If the reliability of a rail system is to be assessed, it is quite important to develop data on the crack initiation and propagation behavior of rail materials and to develop a damage accumulation model which relates constant amplitude laboratory fatigue data with variable amplitude and service simulation fatigue behavior.

Crack propagation data, both constant and variable amplitude, were developed in a previous DOT/TSC program (1)* (Contract No. DOT-TSC-1076). A predictive model for crack growth was also developed. (2)

In task 3 of this program, the problems of crack initiation were assessed, both in terms of the development of critical data and the formulation of a damage model. This report contains the results of the Task 3 efforts.

*References are listed on page 56.

2. RAIL MATERIALS

Two 39-foot sections of new 100-pound/yard rail steel were purchased from the Fritz Rumer Cooke Company for this program. In addition, four shorter sections of used rail material were obtained to provide a cross-section of used rails for a comparison with presently produced standard rail. Background data on the used rail materials are presented in Table 1. Further information on chemistry is included in Reference 3 and an inclusion content in Reference 4.

TABLE 1. USED RAIL MATERIAL BACKGROUND DATA

BCL Rail Number	Source Number	Rail Weight (lbs)	Year Rolled	Characteristics
3	100	85	1920	Low Sulfur/Oxygen Ratio High Inclusion
4	418	130	1929	Low S/O Ratio Low Inclusion
5	VD-2	115	1974	High S/O Ratio Intermediate Inclusion
6	398	130	1929	Intermediate S/O Ratio Intermediate Inclusion

3. EXPERIMENTAL DETAILS

3.1 SPECIMENS

Two specimen geometries were used for the majority of experiments in this program. Both specimen geometries were designed with a 0.25-inch diameter reduced section. The specimens tested at BCL were designed with threaded ends as shown in Figure 1, while the specimens tested at Boeing Commercial Airplane Company (BCAC) were designed with longer smooth ends as shown in Figure 2, to accommodate hydraulic grips. A small number of reduced-size, threaded-end specimens of the type shown in Figure 3 were also designed for transverse rail orientation specimens.

The longitudinal rail specimens were removed from three different locations within the rail cross-section. The center head specimens were taken from 3/4-inch square blanks of material centered on the midplane on the rail head (see Figure 4). The intermediate head specimens were taken from blanks centered 1/2-inch from the rail midplane and one-inch from the upper rail surface (see Figure 5). The surface head specimens were taken from blanks taken as near the side surfaces of the rail as possible centered in a plane one-inch from the upper rail surface (see Figure 6). The transverse rail head specimen blanks were taken from the rail centered in a plane one-inch from the upper rail surface. Because of the location and orientation within the rail, the transverse specimens were only about 2-1/2 inches long, as previously shown in Figure 3.

The number of each type of specimen produced is detailed in Table 2. An overall total of 254 specimens were produced; 156 of those for testing by BCAC, including 64 used rail specimens.

TABLE 2. RAIL SPECIMEN INVENTORY

Rail	Specimen Type	BCL Specimens	BCAC Specimens
Unused	Center	78	42
	Intermediate	--	20
	Surface	12	30
	Transverse	8	--
Used	Center	--	64 ^(a)
	Total	98	156
	OVERALL TOTAL.....		254

(a) 16 specimens from each of 4 used rails.

3.2 TESTING PROCEDURES

The BCL fatigue crack initiation experiments were conducted in a 20,000-pound capacity electrohydraulic servocontrolled fatigue machine. All BCL tests were performed in strain control at cycling frequencies ranging from 5 to 20 Hz, depending on strain amplitude. Environmental conditions were maintained at 70F and 50-percent relative humidity. Load as a function of time was recorded continuously for most experiments and stress-strain hysteresis loops were recorded at frequent intervals.

The BCAC crack initiation experiments were conducted on an Amsler Vibraphone in load control at a frequency of about 105 Hz. In selected cases, the specimen temperature during testing was monitored; temperatures approaching 150 F were found in short

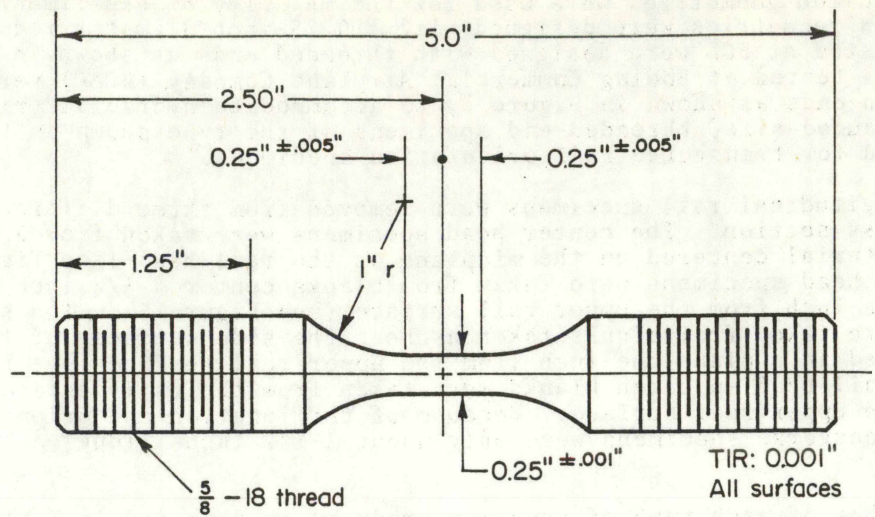


FIGURE 1. BCL UNIAXIAL FATIGUE TEST SPECIMEN

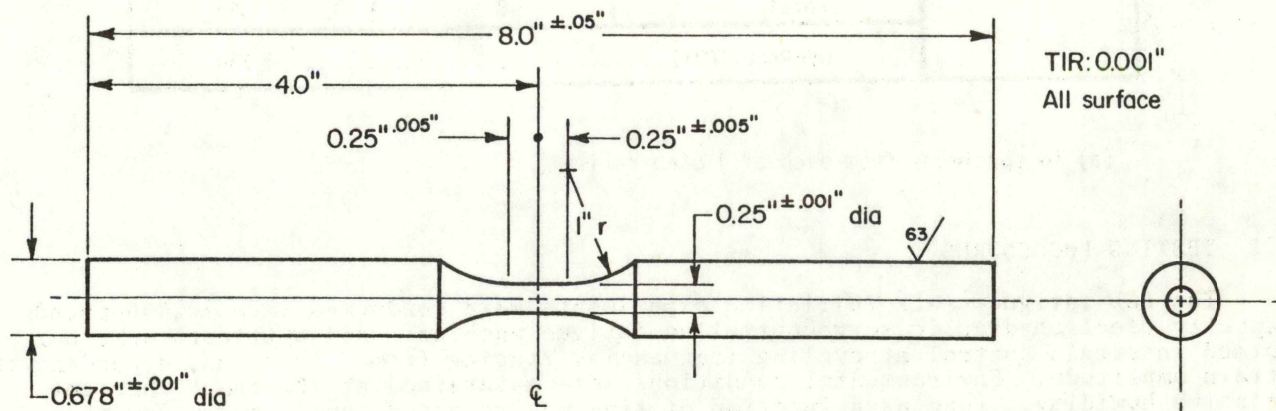


FIGURE 2. BCAC UNIAXIAL FATIGUE TEST SPECIMEN

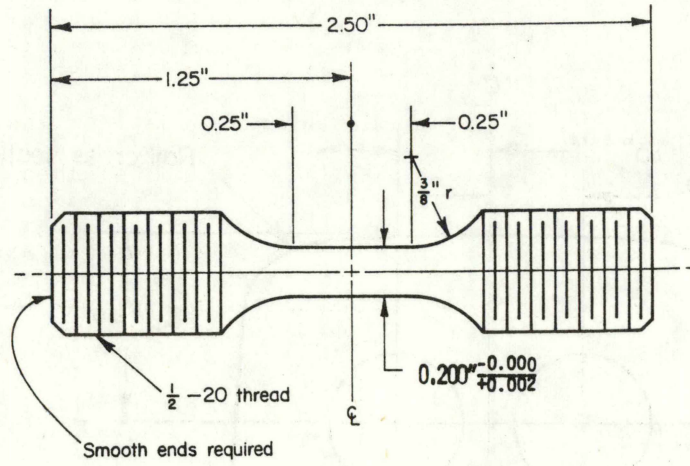


FIGURE 3. TRANSVERSE RAIL UNIAXIAL FATIGUE TEST SPECIMEN

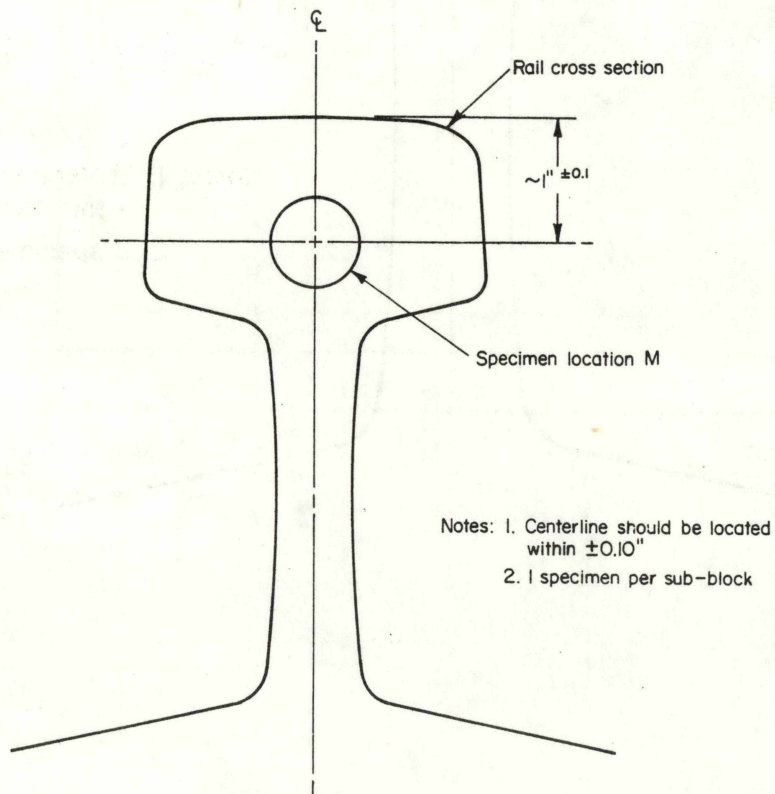


FIGURE 4. CENTER-HEAD SPECIMEN LOCATION

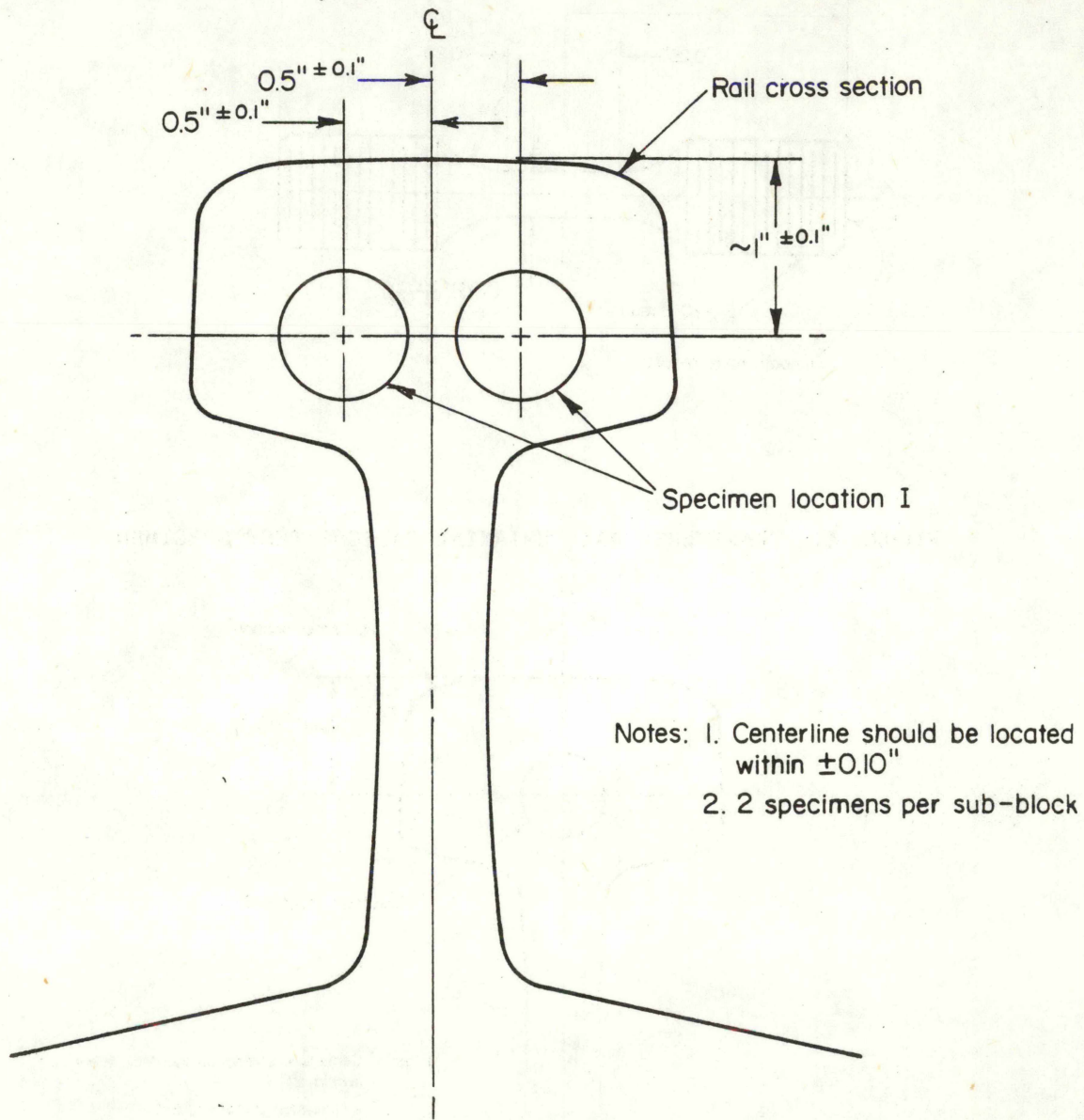


FIGURE 5. INTERMEDIATE SPECIMEN LOCATION

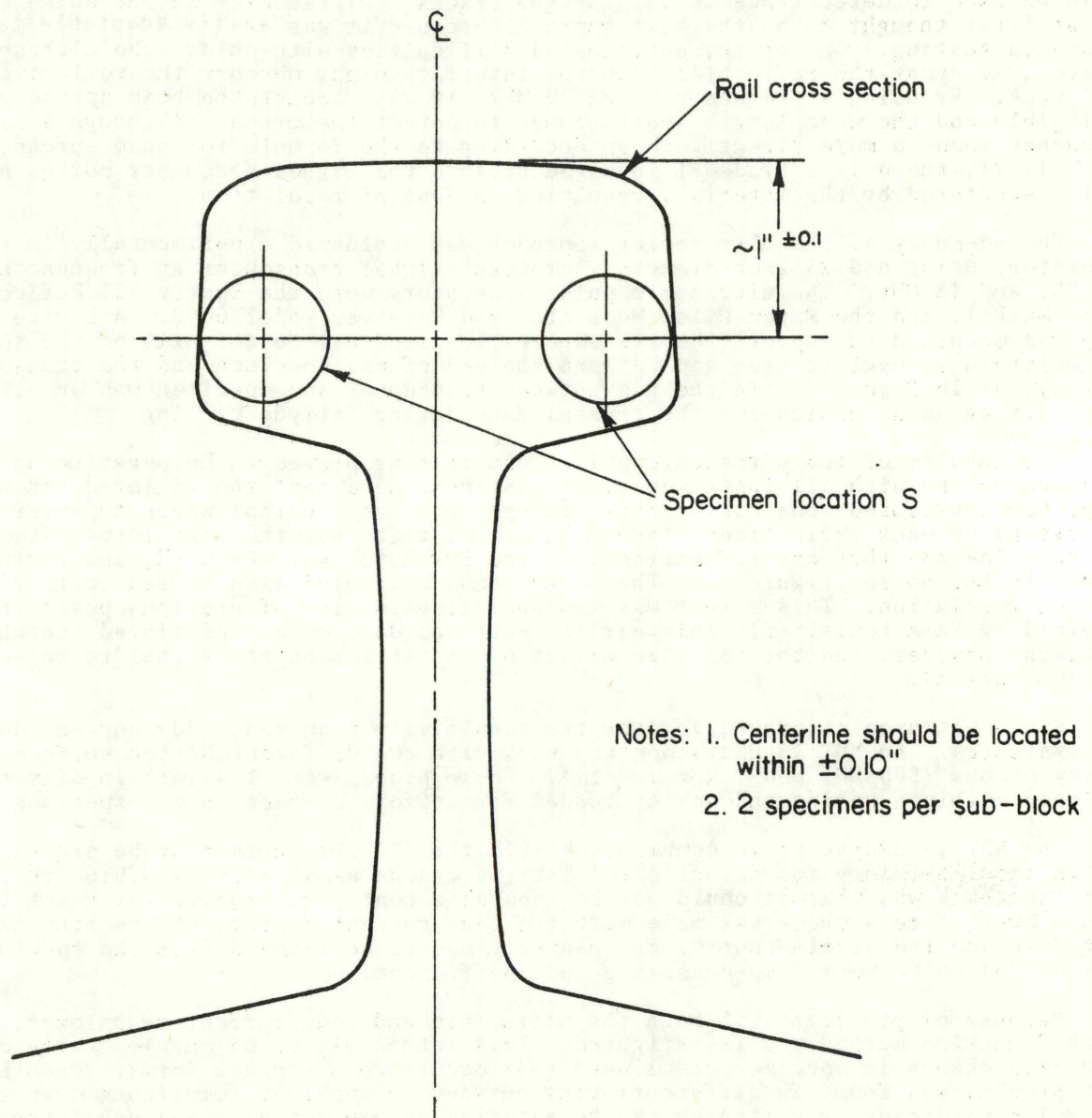


FIGURE 6. SURFACE SPECIMEN LOCATION

life tests ($N_i \approx 100,000$ cycles) while temperatures did not exceed 100 F for the long life tests ($N_i > 1,000,000$ cycles).

3.3 CRACK INITIATION DETECTION

It was a primary objective in the BCL tests performed in this program to develop some technique for detection of small fatigue cracks in the laboratory specimens tested under constant amplitude conditions. Detection of cracks less than 0.04 inch (1 mm) deep was considered possible and desirable. This would provide a less ambiguous definition of crack initiation, necessary for a smooth transition from crack initiation analysis to crack propagation analysis in the reliability study.

Originally, it was considered likely that either ultrasonics or eddy-currents could be used to detect these small fatigue cracks. Ultrasonics in the pulse echo mode was at first thought to be the best approach because it was easily adaptable to automated testing. One of the anticipated difficulties with pulse-echo ultrasonics, however, was that the reflection from the interface might obscure the reflection from the crack. By using a frequency above 10 MHz, it was thought the beam spread would be negligible and the wave length small enough to detect the crack. Although a higher frequency means a more directive beam according to the formula for beam spread, $\sin \theta/2 = 1.22\lambda$, there is a tradeoff involved because the higher frequency pulses are more easily scattered by the material, resulting in loss of resolution.

The adequacy of the ultrasonics approach was evaluated experimentally in the laboratory using a 0.25-inch-diameter Aerotech (Alpha) transducer at frequencies of 5, 10, 25, and 43 MHz. The ultrasonic pulse generators were the Sperry 721 Reflectoscope, Sonic Mark I, and the Matec Pulse Modulator and Receiver Model 6600. A Lucite holder grip was machined to support the transducers longitudinal to the axis of the specimen and maintain a specific free gap between the end of the specimen and the transducer crystal, as in Figure 7. In the gap between transducer and specimen was an oil couplet basin acting as a cushion for the crystal face during fatigue cycling.

The results of the ultrasonic pulse-echo testing proved to be negative at all frequencies and with all instruments. It was concluded that the filleted end of the gauge section caused mode conversions (change from longitudinal waves to shear waves) and extensive back reflections of such high amplitude that the signal to noise ratio was very low and that any reflection from the EDM notch was obscured, and virtually hidden in the noise (Figure 7). The high frequencies used also caused scattering and loss of resolution. This result was disappointing in view of previous positive results obtained by NASA Lewis. (5) This earlier work was done on an unfilleted, notched specimen, however, and the negative effect of the fillet on the signal to noise ratio was substantial.

Since ultrasonics proved to lack the sensitivity required, eddy-current detection was evaluated. An NDT 15 Eddyscope was used with two different Nortec surface frequency probes (500 KHz and 2 MHz models). These probes were 1/4-inch in diameter, enclosed within a casing and spring loaded for uniform contact on the specimen.

The NDT 15 Eddyscope in combination with the 500 KHz surface probe proved successful in the laboratory for detection of fatigue cracks as shallow as 0.015 inch. Its major drawback was that it could not be used as a continuous monitor of crack initiation. Every time a check was made with the eddy current system, the machine had to be shut down and the strain control extensometry had to be removed from the specimen. This proved to be very time-consuming and inefficient.

Because of problems with both the ultrasonic and eddy current techniques, a third crack detection method was investigated. This method was based purely on the detection of a change in specimen compliance that occurs when a crack forms. One significant problem was found in differentiating between an apparent compliance change caused by cyclic hardening or softening of the material and an actual compliance change caused by crack formation. It was found, however, through some trial and error experimentation, that nearly all specimens developed a stable stress response to constant amplitude strain cycling by the time each specimen has been subjected to about half the expected cycles to failure. At this point, it was possible to monitor the maximum cyclic stress (actually load was measured but for a constant specimen area on an un-notched specimen, stress can be considered directly proportional to load) and to note small increases or decreases in that maximum stress. If such changes occurred, it was nearly always an indicator that a crack had developed and that failure of the

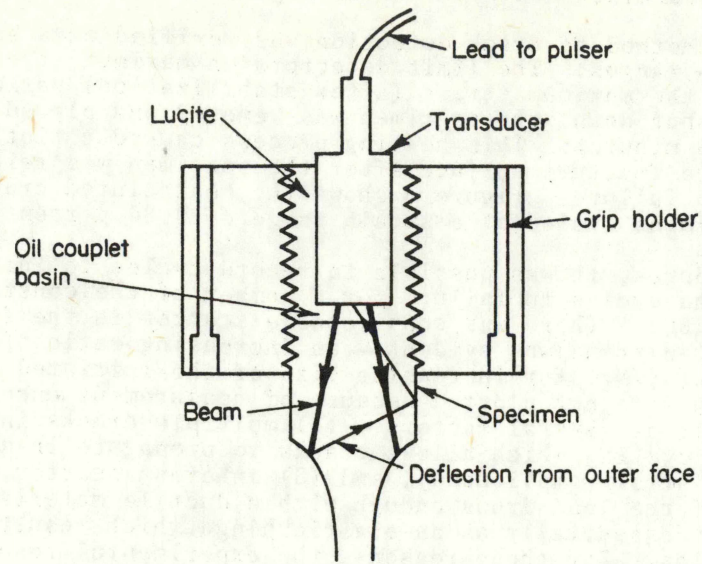


FIGURE 7. ULTRASONIC TRANSDUCER SETUP

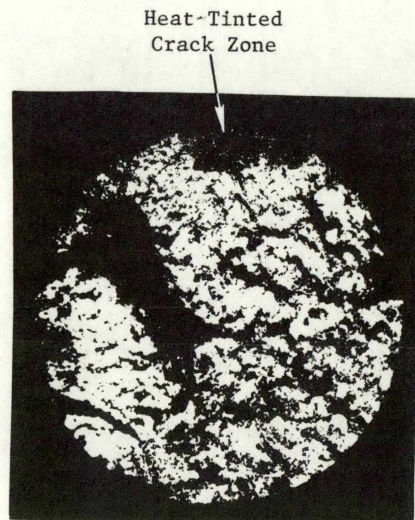


FIGURE 8. HEAT TINTED CRACK INITIATION ZONE ON SPECIMEN 2-11-E

specimen was soon to follow. A decrease in max. stress indicated cracking in the specimen between the clip gauge probes because the compliance of a specimen reduces in the region of a crack which lowers the load for a given strain limit. An increase in max. stress indicated a crack outside the probes of the clip gauge. The large majority of specimens developed cracks between the clip gauge probes.

The specimen compliance method of crack detection was verified on a series of specimens at different strain ranges. The limit detectors on maximum stress were set to shut off the machine when the maximum stress (after stabilization) varied by 2 to 4 percent. After the machine shut down, the specimen was removed and placed in a small furnace at about 700 F for 45 minutes. This heating process caused a tinting of the crack which was visible on the fracture surface after the specimen was reinstalled in the test system and cycled to failure. Figure 8 shows the heat tinted crack initiation on one of the test specimens cycled at a strain range of 0.80 percent.

Through the above procedures, it was possible to record cycles to initiation, the crack depth at initiation, and cycles to failure for a number of the constant strain amplitude tests performed at BCL. There was considerable scatter in the final results (see Figure 9) but the expected trend was evident—an increasing ratio of initiation cycles to propagation cycles (N_i/N_f) for increasing size of the initiated crack. Crack depths below 0.010-inch were not plotted because of measurement uncertainties. Observed scatter is the result of several factors — (1) multiple cracks in some instances (2) strain control cycling which allows cracks to propagate in a semistable manner (especially under low strain amplitudes), and (3) inherent scatter in material behavior. In the extreme, if the load drops enough with a ductile material, it is possible for the crack to act essentially as an elastic hinge which results in unrealistically high N_i/N_f ratios. For these reasons, the experimental results did not permit establishment of a clearly defined relationship between N_i/N_f and crack depth.

In summary, the specimen compliance technique could not be used to precisely identify the point when a small crack of some specific depth has been reached. Too many variables influenced the accuracy of the technique. It could be used, however, to identify an approximate relationship between N_i/N_f and crack depth that could be used to approximate what portion of the total cycles to failure was involved in the initiation of a crack of a given depth. It also was a method of crack initiation monitoring that could be used both by BCL and BCAC. It was, therefore, adopted by both laboratories in this study.

4. TEST RESULTS

4.1 CONSTANT AMPLITUDE EXPERIMENTS

A total of 191 constant amplitude crack initiation experiments were completed in this program. Of this total, 42 were strain-controlled experiments conducted at BCL, while the others were load-controlled experiments conducted at BCAC. All of the BCL experiments were completed on new rail material, while 57 of the BCAC specimens were taken from used rail material. The program involved extensive laboratory testing - approximately 200 million fatigue cycles were applied to generate just the unused rail data.

4.1.1 Unused Rail Data

A direct comparison of data generated in both laboratories was desirable, but that comparison was complicated by the differences in control parameters. In the BCL strain control tests, cyclic softening of the new rail material from its initial monotonic stress-strain response was observed. This behavior is shown in Figures 10, 11, and 12 for center, surface, and transverse rail specimens, respectively. In other words, for a given strain amplitude, the observed maximum stress in individual hysteresis loops decreased from a higher initial monotonic response to a lower, stable maximum stress. A corresponding increase in plastic strain was, of course, seen with the decreasing maximum stress in each specimen. This trend is clearly visible in a series of hysteresis loops reproduced in Figure 13.

In the BCAC load control tests, strain was not monitored, but it is evident from Figures 10 and 11 that some cyclic softening (under constant stress) should be expected at the stress levels evaluated. With small plastic strains, as were seen in the long-life BCAC tests, this softening behavior remained stable and controlled; but load control tests at higher stress amplitudes would likely have resulted in unconstrained cyclic strain softening (or ratcheting) of the specimen, leading to tensile failures rather than fatigue failures. Since only medium to long life tests were performed at BCAC, this ratcheting phenomenon did not occur.

From the cyclic stress-strain data developed in the BCL tests, it was possible to predict the stable strain response of the BCAC tests and to equate test results from the two sources. This was done through calculation of an equivalent strain parameter previously analyzed at BCL. (6) This parameter is similar in form to that originally developed by Walker, (7) but it was modified along the lines suggested by Smith, et al. (8) to define ϵ_{eq} as follows:

$$\epsilon_{eq} = (\Delta\epsilon)^m (\sigma_{max})^{1-m} \quad (1)$$

where $\Delta\epsilon$ = stable strain range

σ_{max} = maximum stable stress

E = elastic modulus

m = constant for a material

In order to compute equivalent strains using Equation (1), it is obviously necessary to know the correct values for each constituent term in the expression. In the BCL strain control tests $\Delta\epsilon$ was controlled, σ_{max} was measured (at the point of stable stress response), and an average E was computed from a series of monotonic stress-strain curves. In the BCAC load control tests σ_{max} was controlled, but $\Delta\epsilon$ and E had to be estimated from monotonic and cyclic stress-strain data. Values of $\Delta\epsilon$ were computed by using the following equations which approximated the cyclically stable stress-strain response of the longitudinally oriented rail specimens:

$$\Delta\epsilon = \frac{2S_a}{E}, \quad 0 \leq \Delta\epsilon \leq \Delta\epsilon(1), \quad (2a)$$

$$\Delta\epsilon = 2 \left(\frac{S_a}{K_1} \right)^{1/n_1}, \quad \Delta\epsilon(1) < \Delta\epsilon \leq \Delta\epsilon(2), \quad (2b)$$

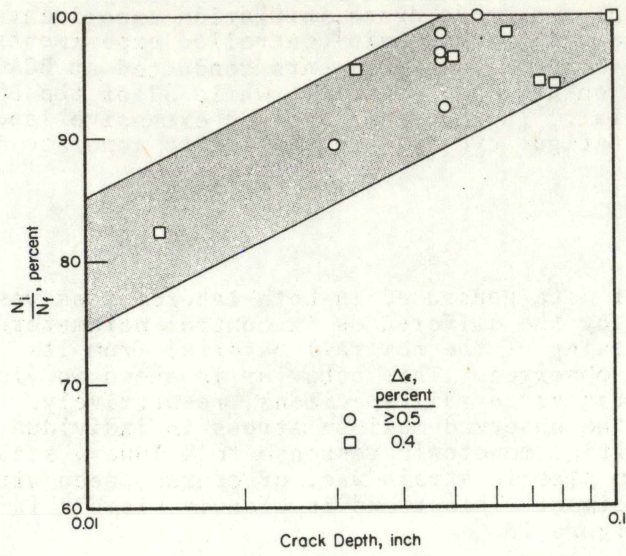


FIGURE 9. RATIO OF INITIATION CYCLES TO TOTAL FAILURE CYCLES AS A FUNCTION OF CRACK DEPTH

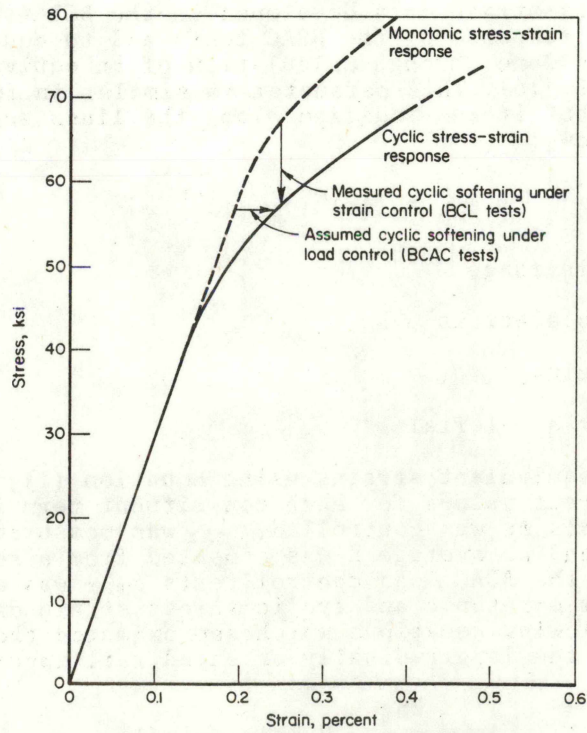


FIGURE 10. MONOTONIC AND CYCLIC STRESS-STRAIN BEHAVIOR OF CENTER-HEAD RAIL SPECIMENS

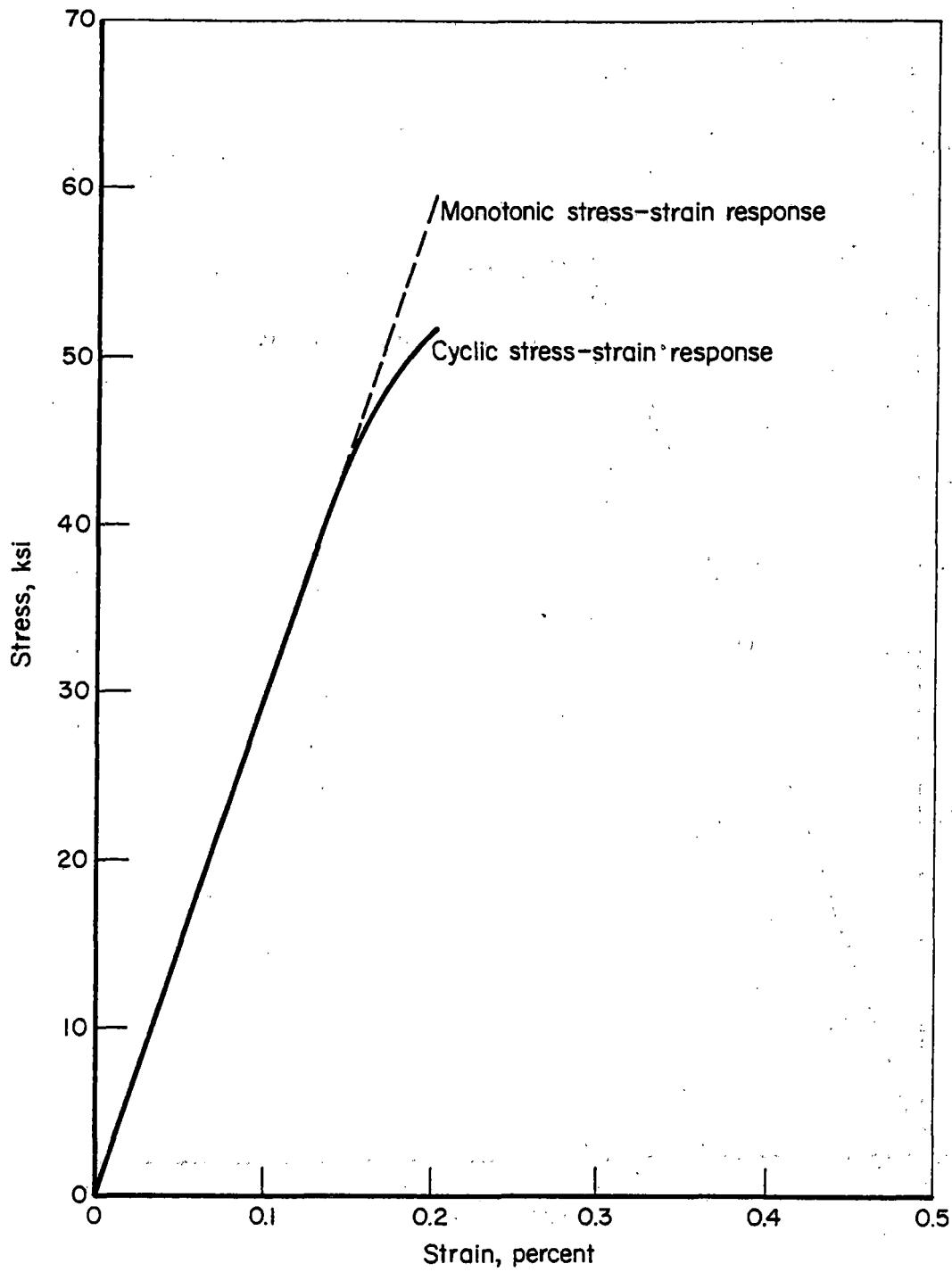


FIGURE 11. MONOTONIC AND CYCLIC STRESS-STRAIN BEHAVIOR OF SURFACE-HEAD RAIL SPECIMENS

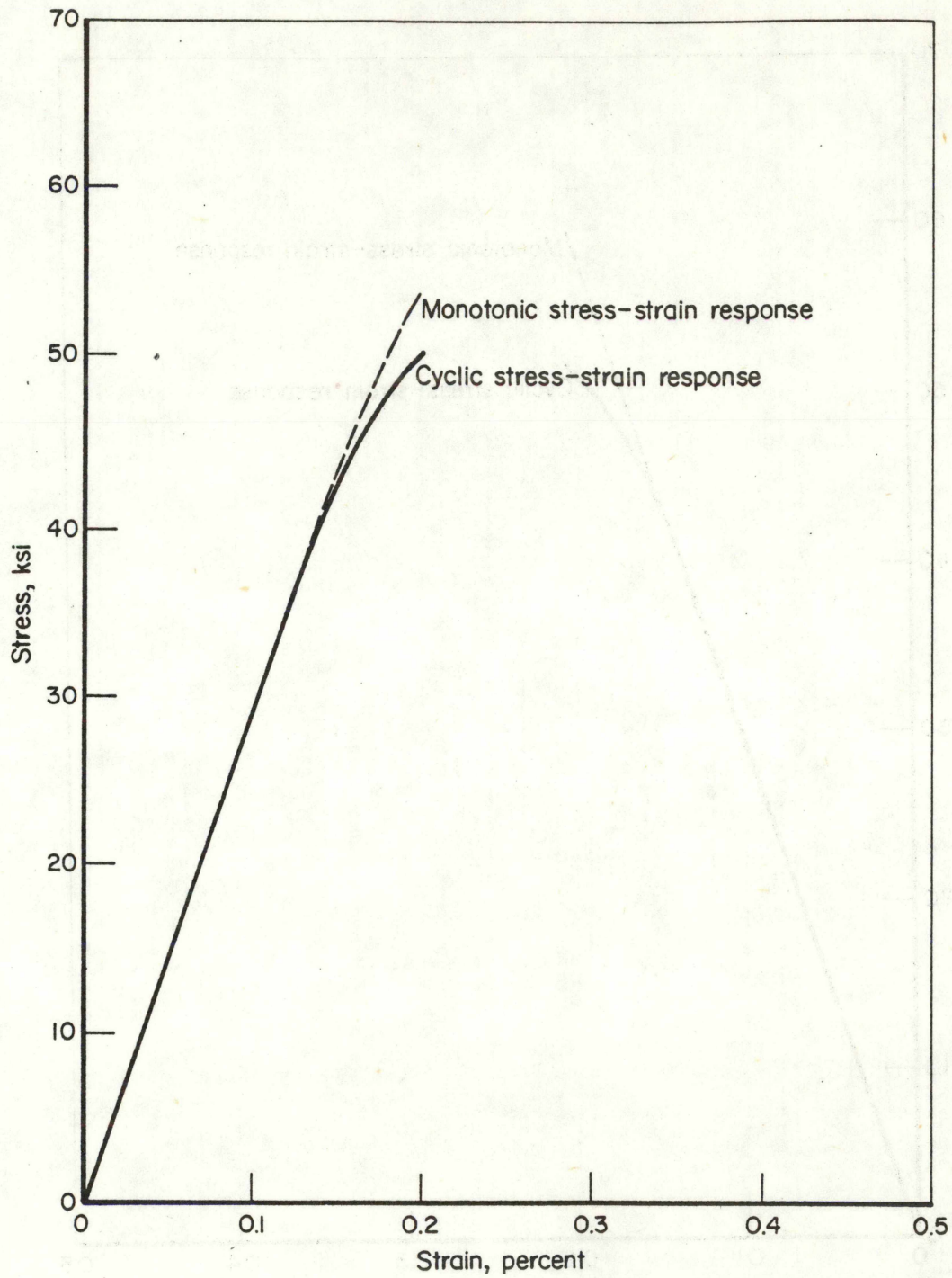


FIGURE 12. MONOTONIC AND CYCLIC STRESS-STRAIN BEHAVIOR ON TRANSVERSE-HEAD RAIL SPECIMENS

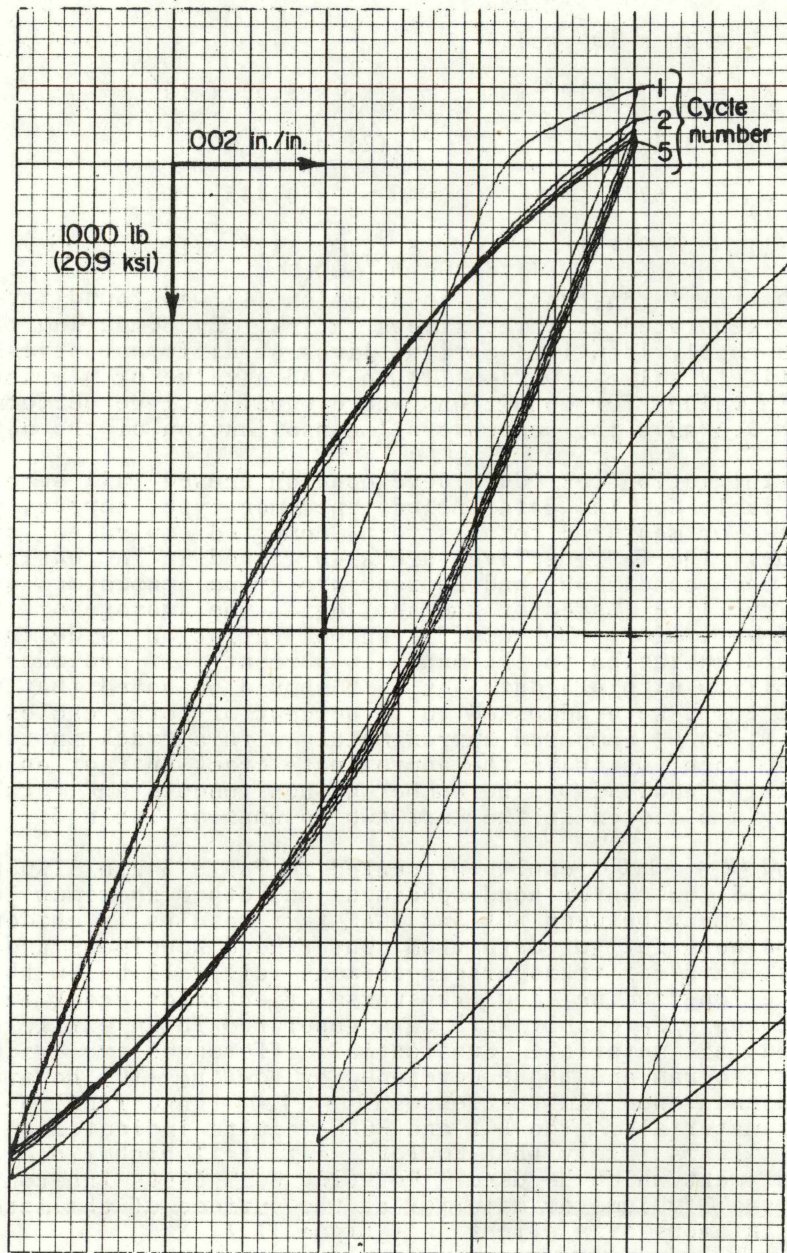


FIGURE 13. STRESS-STRAIN HYSTERESIS LOOPS FOR SPECIMEN 1-6-E THROUGH FIRST FIVE CYCLES AT 0.8-PERCENT STRAIN RANGE

$$\Delta\epsilon = 2 \left(\frac{S_a}{K_2} \right)^{1/n_2}, \Delta\epsilon(2) < \Delta\epsilon, \quad (2c)$$

where K_1 and K_2 = strength coefficients

n_1 and n_2 = strain hardening exponents

$\Delta\epsilon(1)$ and $\Delta\epsilon(2)$ = specific values of $\Delta\epsilon$ that denote break points in the tri-log-linear stress-strain curve approximation.

The approximate values for the constants in the Equation (2) series were found as follows for the new rail material:

$$\begin{aligned} E &= 29 \times 10^3 \text{ ksi} \\ K_1 &= 3.43 \times 10^3 \text{ ksi} & K_2 &= 8.05 \times 10^2 \text{ ksi} \\ \Delta\epsilon(1) &= 2.7 \times 10^{-3} & \Delta\epsilon(2) &= 4.0 \times 10^{-3} \\ n_1 &= 0.677 & n_2 &= 0.443 \\ S_a(1) &= 39.1 \text{ ksi} & S_a(2) &= 51.3 \text{ ksi} \end{aligned}$$

A value for the material constant, m , in Equation (1) was found through an examination of the BCAC data generated at three stress ratios. By comparing the stress conditions which provided nearly identical fatigue lives at different stress ratios, it was possible to iteratively solve Equation (1) to find a value of m which provided equal equivalent strain values for conditions where equal fatigue performance had been found. A value of $m = 0.6$ gave the best overall consolidation of the data.

All of the crack initiation test data developed on unused rail samples in this program are listed in Table 3. The data include specimen type, source, stress ratio, maximum stress, computed or measured total strain, computed equivalent strain and specimen identification. The fatigue lives are also listed in increasing order of cycles to failure for each condition, and appropriate group statistics are presented including average fatigue life (based on the antilog of the average of the log lives), and the coefficient of variation. The coefficient of variation is defined as the ratio of sample standard deviation to the mean (in percent); it provides an indication of the relative variability within a data set. It should be noted that the cycles to initiation for the BCL tests were adjusted to 94 percent of total cycles to failure because that ratio of N_i to N_f compared approximately with a crack initiation crack depth of 0.030 to 0.040 inch, which is the approximate crack initiation crack size chosen for the reliability analysis. The number of non-runouts and total specimens tested in each category are listed in the last two columns of Table 3.

The fully reversed ($R = -1.0$) results presented in Table 3 are displayed graphically in Figures 14 and 15 for center head specimens and other specimen locations, respectively. Good agreement between BCL and BCAC test results is evident. There is also close agreement between fatigue data from center head specimens and surface and intermediate specimens; data for transverse specimens fall well below those for other orientations. Both the longitudinal and transverse orientation crack initiation fatigue test results compare favorably with data generated in an earlier program at BCL (9) on a hot rolled rail material. Substantial differences are evident between the data developed in this program and those developed by Fowler, (10) however. For example, his indicated endurance limit stresses ($R = -1.0$) range from about 52 to 62 ksi for six different rail materials. The BCL and BCAC results indicated endurance limit stresses below 50 ksi. It is likely that Fowler data fall higher because of the rotating beam test equipment which he used. Rotating beam tests inherently apply maximum stresses to a small volume of material at the surface of the material, which commonly leads to the infamous size effect in fatigue. (11)

4.1.2 Used Rail Data

The crack initiation tests on the used rail materials were conducted at BCAC. Including specimens used to set stress levels, there were 57 tests completed on four different used rails. The tests were performed in load control at a stress ratio of 0.10 with maximum stress levels ranging from 65 ksi to 105 ksi. Five to seven tests

TABLE 3. COMPLETE LISTING OF ALL BCL AND BCAC CONSTANT AMPLITUDE CRACK INITIATION TEST DATA ON UNUSED RAILS

Specimen Type	Source	Stress Ratio, R	Maximum Stress, σ_{max}	Computer or Measured Total Strain, $\Delta\epsilon\%$	Computed Equivalent Strain $\epsilon_{eq} \times 10^{-3}$	Specimen Identification	Ranked Fatigue Life n_i	Average Life Based on Log. n_i	Coefficient of Variation, %	Number of Tests	
										Non-Runout	Total
Center	BCL	-1.00	66.8	0.80	4.86	1-6-E 2-11-E	10775 11770	11,260	0.7	2	2
	BCL		67.0	0.70	4.49	2-3-C	14330	14,330	-	1	1
	BCL		56.3	0.50	3.42	2-2-C 1-12-C 2-12-E	49710 57610 77690	60,595	2.1	3	3
	BCAC		54.0	0.448	3.15	2-11-D 1-6-D 2-10-B 2-13-B 2-5-B	60000 65000 88000 115000 308000	103,982	5.7	5	5
	BCAC		52.0	0.412	2.95	1-7-B	104000	104,000	-	1	1
	BCL		51.4	0.40	2.89	1-2-A 1-11-C 1-10-A 1-2-E 1-5-E 1-5-A 2-3-E	92850 163800 183300 187800 234700 246800 924600	223,615	5.7	7	7
	BCAC		50.0	0.388	2.80	1-10-B 2-11-B 2-24-D 1-3-D 1-6-B 2-3-B 1-7-D 2-8-D	256000 328000 431000 438000 610000 973000 3026000 5087000R	601,446	6.3	7	8

TABLE 3. (Continued)

Specimen Type	Source	Stress Ratio, R	Maximum Stress, σ_{max}	Computer or Measured Total Strain, $\Delta\epsilon\%$	Computed Equivalent Strain $\epsilon_{eq} \times 10^{-3}$	Specimen Identification	Ranked Fatigue Life n_i	Average Life Based on Log, n_i	Coefficient of Variation, %	Number of Tests	
										Non-Runout	Total
Surface	BCL		49.2	0.375	2.73	2-9-C 1-1-C 1-1-E 1-5-C 1-1-A 1-12-A 2-7-C 1-11-E 2-9-E 2-5-A 2-7-A 2-4-A 1-2-C	286300 322700 398700 1241000 1260000 1401000 5000000R 5000000R 5000000R 5000000R 5870000R 7060000R 8100000R	657,367	5.6	6	13
	BCAC		49.0	0.376	2.73	2-4-B	5078000R	---	---	0	1
	BCL		45.3	0.35	2.53	1-10-E 2-2-A 1-8-E	1680000R 4100000R 14200000R	---	---	0	3
	BCAC		46.0	0.343	2.52	2-7-D	5187000R	---	---	0	1
	BCL		44.2	0.33	2.42	1-4-E	5870000R	---	---	0	1
	BCL		42.5	0.30	2.25	2-12-C	7250000R	---	---	0	1
	BCAC	-1.00	54.0	0.448	3.15	1-6-D 2-3-B 1-6-B 1-10-B	91000 102000 120000 167000	116,784	2.3	4	4
	BCAC		52.0	0.412	2.95	2-7-B	334000	334,000	---	1	1
	BCL		51.6	0.40	2.89	2-8-C 2-10-E 2-10-C	127870 173940 179290	158,577	1.6	3	3

TABLE 3. (Continued)

Specimen Type	Source	Stress Ratio, R	Maximum Stress σ_{max}	Computer or Measured Total Strain, $\Delta\epsilon\%$	Computed Equivalent Strain $\epsilon_{eq} \times 10^{-3}$	Specimen Identification	Ranked Fatigue Life n_i	Average Life Based on Log, n_i	Coefficient of Variation, %	Number of Tests	
										Non-Runout	Total
Inter-mediate	BCAC		50.0	0.388	2.80	1-8-E 1-10-D 2-8-D 2-11-D 1-5-D 2-13-B	303000 309000 358000 712000 5080000R 5100000R	393,044	3.1	4	6
	BCL		49.1	0.375	2.73	2-8-A 2-10-A 2-7-D	528100 1663800 1520000R	937,365	5.9	2	3
	BCAC		48.0	0.365	2.66	1-5-B	5116000R	---	---	0	1
	BCAC	-1.00	54.0	0.448	3.15	2-12-D1 2-13-D1	79000 107000	91,940	1.9	2	2
	BCAC		50.0	0.388	2.80	1-13-B2 1-13-B1 1-13-D2 2-12-B1	589000 645000 1314000 1324000	901,653	3.2	4	4
Trans-verse	BCAC		49.0	0.376	2.73	2-12-B2	2816000	2816,000	---	1	1
	BCL	-1.00	50.1	0.40	2.86	1-3-T 1-1-T	36848 54285	44,725	2.6	2	2
	BCL		48.7	0.375	2.72	2-4-T 1-2-T 2-3-T	42770 46568 95579	57,526	4.0	3	3
Center	BCAC	0.10	100.0	0.332	3.37	2-6-B	57000	57,000	---	1	1
	BCAC		95.0	0.308	3.15	1-3-B 2-9-D 1-11-D 2-1-D 2-6-D	66000 107000 144000 154000 177000	122,619	3.3	5	5
	BCAC		90.0	0.284	2.94	1-2-B	294000	294,000	---	1	1

TABLE 3. (Continued)

Specimen Type	Source	Stress Ratio, R	Maximum Stress, σ_{max}	Computer or Measured Total Strain, $\Delta\epsilon\%$	Computed Equivalent Strain $\epsilon_{eq} \times 10^{-3}$	Specimen Identification	Ranked Fatigue Life n_i	Average Life Based on Log, n_i	Coefficient of Variation, %	Number of Tests	
										Non-Runout	Total
Surface	BCAC	0.10	85.0	0.264	2.75	1-4-D 1-4-B 2-3-D 2-1-B 2-7-B 2-10-D	220000 274000 495000 651000 771000 806000	484,608	4.1	6	6
	BCAC		83.0	0.258	2.69	2-9-B	3384000	3384,000	---	1	1
	BCAC		69.0	0.214	2.23	1-10-D	5068000R	---	---	0	1
	BCAC		100.0	0.332	3.37	1-9-D	62000	62,000	---	1	1
	BCAC		95.0	0.308	3.15	2-6-D 1-8-D 2-11-B 2-8-B	108000 117000 118000 149000	122,087	1.2	4	4
Inter-mediate	BCAC	0.10	85.0	0.264	2.75	1-11-D 1-3-B 2-3-D 1-9-B	423000 589000 861000 2311000	839,102	5.4	4	4
	BCAC		75.0	0.233	2.43	2-9-D	5026000R	---	---	0	1
	BCAC		95.0	0.308	3.15	1-1-B1 2-13-D2	51000 72000	60,597	2.2	2	2
	BCAC		85.0	0.264	2.75	2-12-D2 1-10-1 1-1-B2 2-2-D1	112000 177000 999000 2458000	469,715	11.1	4	4
Center	BCAC	0.50	80.0	0.248	2.59	1-11-B1	5048000R	---	---	0	1
	BCAC		125.0	0.216	2.84	2-5-D 1-9-D 1-12-D 1-9-B 1-12-B	102000 143000 167000 209000 210000	160,621	2.5	5	5

TABLE 3. (Continued)

Specimen Type	Source	Stress Ratio, R	Maximum Stress, σ_{max}	Computer or Measured Total Strain, $\Delta\epsilon\%$	Computed Equivalent Strain $\epsilon_{eq} \times 10^{-3}$	Specimen Identification	Ranked Fatigue Life n_i	Average Life Based on Log, n_i	Coefficient of Variation, %	Number of Tests	
										Non-Runout	Total
Surface	BCAC		115.0	0.198	2.62	1-5-D 1-8-B 1-8-D 1-2-D 1-5-B 2-8-B	338000 685000 1716000 2371000 3800000 4498000	1082,621	7.0	6	6
	BCAC	0.50	125.0	0.216	2.84	2-10-B 2-6-B 2-7-D 1-7-D	81000 157000 183000 315000	164,546	4.7	4	4
	BCAC		115.0	0.198	2.62	1-3-D 2-10-D 1-7-B 2-9-B	355000 391000 839000 2567000	739,432	6.8	4	4
Intermediate	BCAC	0.50	125.0	0.216	2.84	1-1-D2 2-2-B1	254000 326000	287,757	1.4	2	2
	BCAC		115.0	0.198	2.62	1-13-D1 1-11-B2 2-2-D2	984000 1832000 5059000R	1342,642	3.1	2	3
	BCAC		110.0	0.190	2.50	2-2-B2	5058000R	---	---	0	1

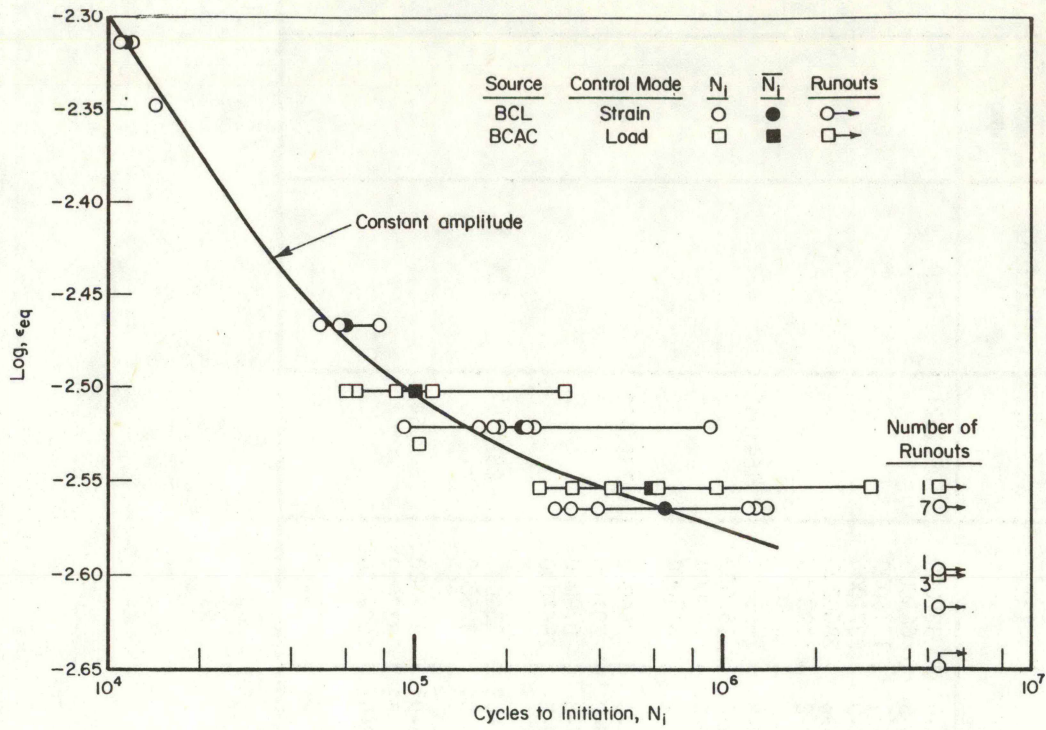


FIGURE 14. FATIGUE LIFE VS. EQUIVALENT STRAIN FOR CENTER-HEAD RAIL SPECIMENS

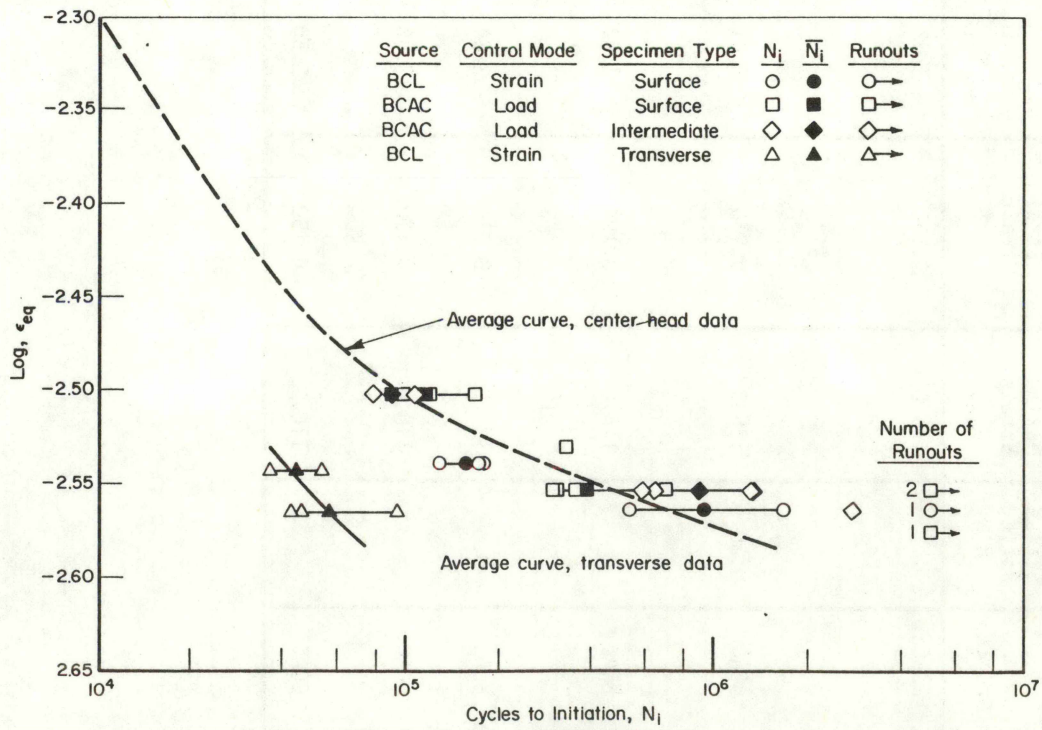


FIGURE 15. FATIGUE LIFE VS. EQUIVALENT STRAIN FOR SURFACE-, INTERMEDIATE-, AND TRANSVERSE-HEAD RAIL SPECIMENS, $R=1.0$

were completed at each of two stress levels for each rail material. The reduced data are presented in Table 4. The variability in fatigue performance compared to the baseline data on unused rail material is shown in Figure 16. The data are plotted in terms of maximum stress rather than equivalent strain since cyclic stress-strain data on the used rail materials were not generated.

Two used rail materials performed far below crack initiation fatigue life trends previously established for the unused rail. These were rails produced in the 1920's. One rail performed similarly to the new, unused rail; it was a vacuum-degassed rail produced since 1970. The fourth rail, which performed somewhat better than the unused rail, was also produced in the 1920's. No correlation was evident between fatigue performance and either sulfur to oxygen ratio or inclusion content of the rail material.

4.2 PERIODIC OVERSTRAIN EXPERIMENTS

The objective of these experiments was to determine the extent to which periodic overstrains would affect the fatigue resistance of the rail steel in the regime of the constant amplitude fatigue limit and below. If it were assumed that all cycles experienced by a rail material below its constant amplitude fatigue limit are non-damaging, a periodic overstrain should not cause failure until the total number of overstrain cycles is equal to the cyclic life of a virgin specimen subjected to constant amplitude cycling at the overstrain level. A comparison of actual cycles to failure and this hypothetical fatigue life is made in Table 5. It is obvious that the small amplitude cycles below the constant amplitude endurance limit were actually quite damaging when combined with periodic overstrains. In fact, if the small amplitude cycles to failure are plotted on an equivalent strain basis, excluding the overload cycle, the endurance limit essentially vanishes (or is reduced appreciably). This is shown in Figure 17 where the overstrain data are plotted relative to the constant amplitude baseline crack initiation curve. Elimination of the constant amplitude endurance limit through periodic overstrains has been observed previously by Brose. (13)

Figure 17 does not clearly illustrate the relative damage caused by the overstrain and small amplitude cycles. Table 6 was constructed in an effort to evaluate the extent of damage caused by the large and small amplitude strain cycles; cycles to failure are noted, along with the number of overstrain cycles endured. The number of overstrain cycles were divided by the average cycles to failure under a constant strain range of 0.80 percent (11980 cycles), to compute a percent of damage caused by the large cycles (assuming the linear damage theory as developed by Miner is valid). (12) The number of small amplitude cycles are also listed. Theoretically, according to the linear damage hypothesis, the balance of damage not caused by the large overstrain cycles (100 percent = total damage of failure) should have been caused by the small strain cycles. If this were true, the damage per small cycle could be computed as follows:

$$\Delta D_{\text{small}} = 100 - \Delta D_{\text{large}}, \% \quad , \quad (3)$$

$$\frac{\Delta D_{\text{small}}}{\text{cycle}} = \frac{\Delta D_{\text{small}}}{N_{\text{small}}}, \%/\text{cycle} \quad , \quad (4)$$

where ΔD_{small} = percent of damage caused by small cycles

ΔD_{large} = percent of damage caused by large cycles

N_{small} = number of small cycles.

Values for Equation (4) are presented in the last column of Table 6 for each overstrain specimen.

If the damage process were indeed linear, it would have been expected that the damage/cycle for all four tests at the two different small strain cycle levels would have been equal, or nearly so (taking into account normal fatigue data variability). Differences do exist, however, which suggest some history dependence within the damage process. The history dependence is most evident for the very small strain range tests (0.3 percent). There are two readily identifiable explanations of this phenomenon, neither of which appear to be completely satisfactory, or readily applied to a complex stress history.

TABLE 4. SUMMARY OF USED RAIL FATIGUE TEST RESULTS

BCL Rail Number and Source Number

	MAXIMUM STRESS, ksi	3 (100) AVERAGE FATIGUE LIFE, CYCLES	COEFFICIENT OF VARIATION, CYCLES	MAXIMUM STRESS, ksi	4 (418) AVERAGE FATIGUE LIFE, CYCLES	COEFFICIENT OF VARIATION, CYCLES	MAXIMUM STRESS, ksi	5 (VD-2) AVERAGE FATIGUE LIFE, CYCLES	COEFFICIENT OF VARIATION, CYCLES	MAXIMUM STRESS, ksi	6 (398) AVERAGE FATIGUE LIFE, CYCLES	COEFFICIENT OF VARIATION, CYCLES
Stress Level 1 $N_f \sim 10^5$ (5 tests/rail)	85	128,800	1.9	85	56,230	2.3	95	102,300	4.2	105	85,110	1.3
Stress Level 2 $N_f \sim 10^6$ (7 tests/rail)	75	616,600	2.2	65	489,800	12.5	85	478,600	8.1	95	354,800 ^a	3.4 ^a

(a) One very low test value excluded with $N_f = 10,000$ cycles.

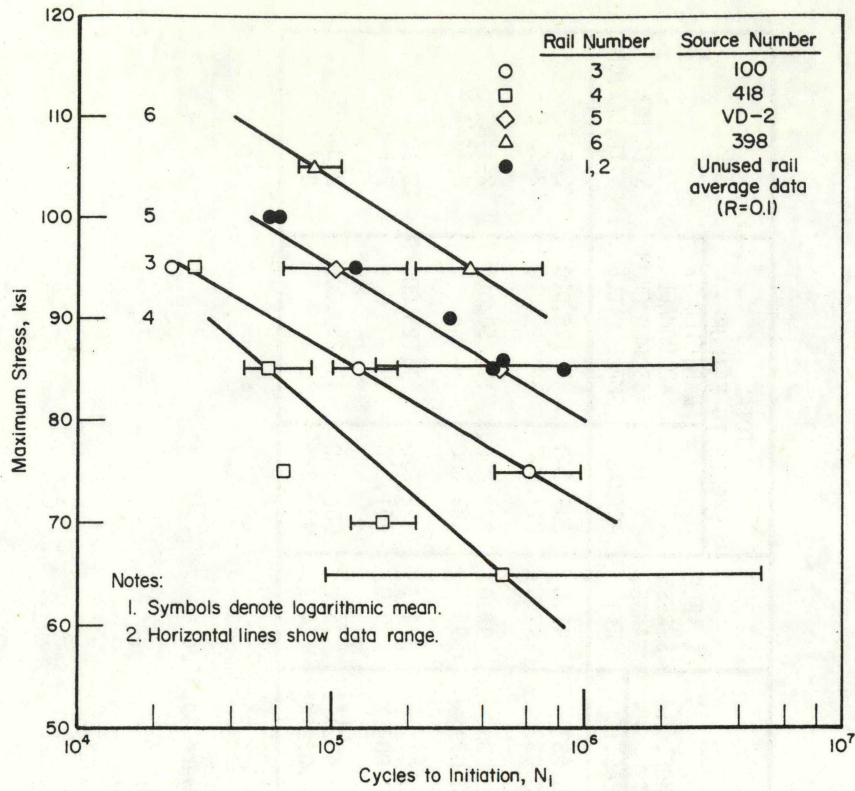


FIGURE 16. FATIGUE LIFE TRENDS FOR USED RAIL MATERIAL

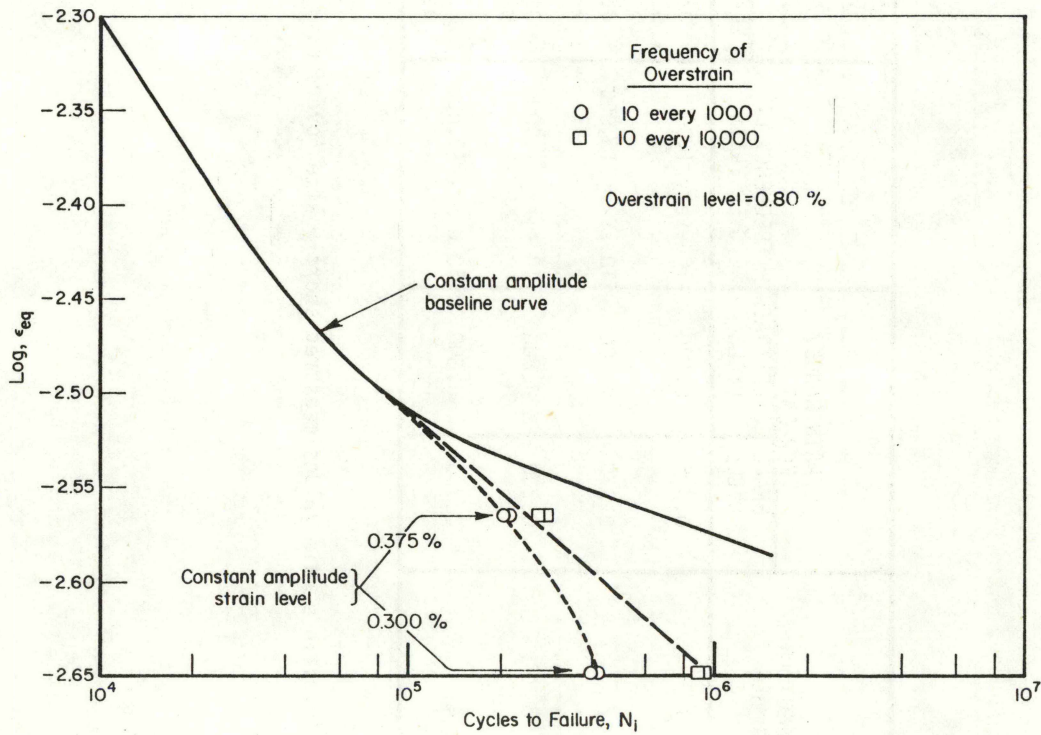


FIGURE 17. PERIODIC OVERSTRAIN FATIGUE TEST RESULTS

TABLE 5. PERIODIC OVERSTRAIN TEST RESULTS ON NEW RAIL MATERIAL

CONDITION NUMBER	STRAIN RANGE, PERCENT		FREQUENCY OF OVERSTRAIN	STRAIN RANGE, PERCENT		STABLE STRESS RANGE, ksi	TOTAL CYCLES TO FAILURE		SPECIMEN IDENTIFICATION
	SMALL CYCLE	OVERSTRAIN CYCLE		PERCENT			ACTUAL	EXPECTED IF NO DAMAGE ASSUMED FROM SMALL CYCLE	
				ELASTIC	PLASTIC				
1	0.375	0.800	10 every 1,000	0.338	0.037	93.8	209,240	1,125,000	2-5-C 2-10-E
				0.342	0.033	91.2	217,600		
2	0.375	0.800	10 every 10,000	0.345	0.030	98.0	270,200	11,250,000	2-1-A 2-12-A
				0.346	0.029	93.5	289,400		
3	0.300	0.800	10 every 1,000	0.289	0.011	79.2	422,820	1,125,000	2-10-C 2-8-E
				0.296	0.004	79.0	401,270		
4	0.300	0.800	10 every 10,000	0.268	0.032 ^(a)	76.2	900,700	11,250,000	2-3-A 2-7-E
				0.271	0.029 ^(a)	74.9	930,785		

(a) Plastic strain values measured shortly after overstrain cycles were applied.

TABLE 6. COMPUTATION OF RELATIVE DAMAGE CAUSED BY LARGE AND SMALL CYCLES IN PERIODIC OVERSTRAIN

CONDITION	CYCLES TO FAILURE, N_f	OVERSTRAIN CYCLES, ΔD_{Large}	OVERSTRAIN CYCLES, $\Delta D_{Large}^{(a)}$	AMPLITUDE CYCLES, N_{Small}	COMPUTED INCREMENT OF DAMAGE PER SMALL CYCLE $\Delta D_{Small}^{(b)}$ $\times 10^{-4}$, % $\frac{\Delta D_{Small}}{\text{Cycle}}$
1	209,240	2,090	17.4%	207,140	3.99
	217,600	2,170	18.1%	215,430	3.80
2	270,200	270	2.25%	269,930	3.62
	289,400	289	2.41%	289,111	3.38
3	422,820	4,220	35.2%	418,600	1.55
	401,270	4,010	33.5%	397,260	1.67
4	900,700	900	7.51%	899,800	1.03
	930,785	930	7.76%	929,850	0.99

(a) $N_f = 11,980$ at $\Delta \epsilon = .80\%$

(b) 100% damage equals failure.

The first explanation is based on a plastic strain accumulation damage hypothesis as investigated by a number of researchers. (14,15) Along this vein, it could be hypothesized that a certain number of large strain cycles were required to cyclically soften the material to the point where plastic strain damage began to develop at the lower strain range as well. Some simple calculations suggest that this is at least plausible, as is demonstrated in Table 7. Since the material does undergo a gradual softening when subjected to cyclic plastic deformation, it is not unreasonable to assume that it would take longer to soften to a level where significant plasticity was experienced at 0.3 percent strain range, than at 0.375 percent. Table 7 suggests that this difference in the required number of large cycles could have been as great as a factor of ten, from 40 large cycles to 400.

The second explanation for the apparent history effects in the overstrain experiments is based on an initiation-propagation damage concept. With this concept, it can be assumed that only cycles above the constant amplitude endurance limit contribute to the formation and initiation of a fatigue crack; but all cycles, including the small ones, are effective in propagating that crack beyond some "equivalent initial flaw." If this concept has physical meaning, it suggests that very small flaws are subject to propagation by sub-endurance limit strain ranges. For example, if it is assumed that the small cycles listed in Column 4 of Table 7 effectively represent initiation cycles, it is evident that N_i/N_f ratios would be extremely small for a .375 percent strain range (from 1 to 11 percent). If Figure 9 is extrapolated back to such small N_i/N_f values, it suggests initiation crack depths well below 0.001 inch. At present there is very little experimental evidence to support this concept; therefore, it is not a practical method to account for stress history effects.

4.3 VARIABLE STRAIN AMPLITUDE EXPERIMENTS

The objective of these experiments was to develop a collection of variable amplitude fatigue data for simulated rail histories that could be used to assess current linear damage accumulation prediction capabilities.

Three different spectra were used in the variable amplitude experiments. These spectra were derived from cumulative probability curves of wheel rail loads measured for four different railroads. These curves are shown in Figure 18. The most severe

TABLE 7. COMPARISON IN NUMBER OF NONDAMAGING SMALL CYCLES IN PERIODIC OVERLOAD EXPERIMENTS

CONDITION	LOWER STRAIN LOAD, %	NUMBER OF LARGE CYCLES REQUIRED TO SOFTEN MATERIAL TO LEVEL WHERE PLASTIC STRAIN OCCURS AT LOWER STRAIN LEVEL	NUMBER OF SMALL CYCLES PAST DURING SOFTENING PROCESS	AVERAGE NUMBER OF DAMAGING SMALL CYCLES	AVERAGE DAMAGE PER SMALL CYCLE $\times 10^{-4}$, %
1	0.375	40	3,000	210,420	3.91
2	0.375	40	30,000	249,800	3.91
3	0.300	400	39,000	368,930	1.78
4	0.300	400	390,000	524,830	1.76

* A block of ten large overstrain cycles began each test, therefore small cycles endured after x overstrain cycles = $\frac{(x-10)}{10} \cdot (R)$, where R is the ratio of small to large cycles.

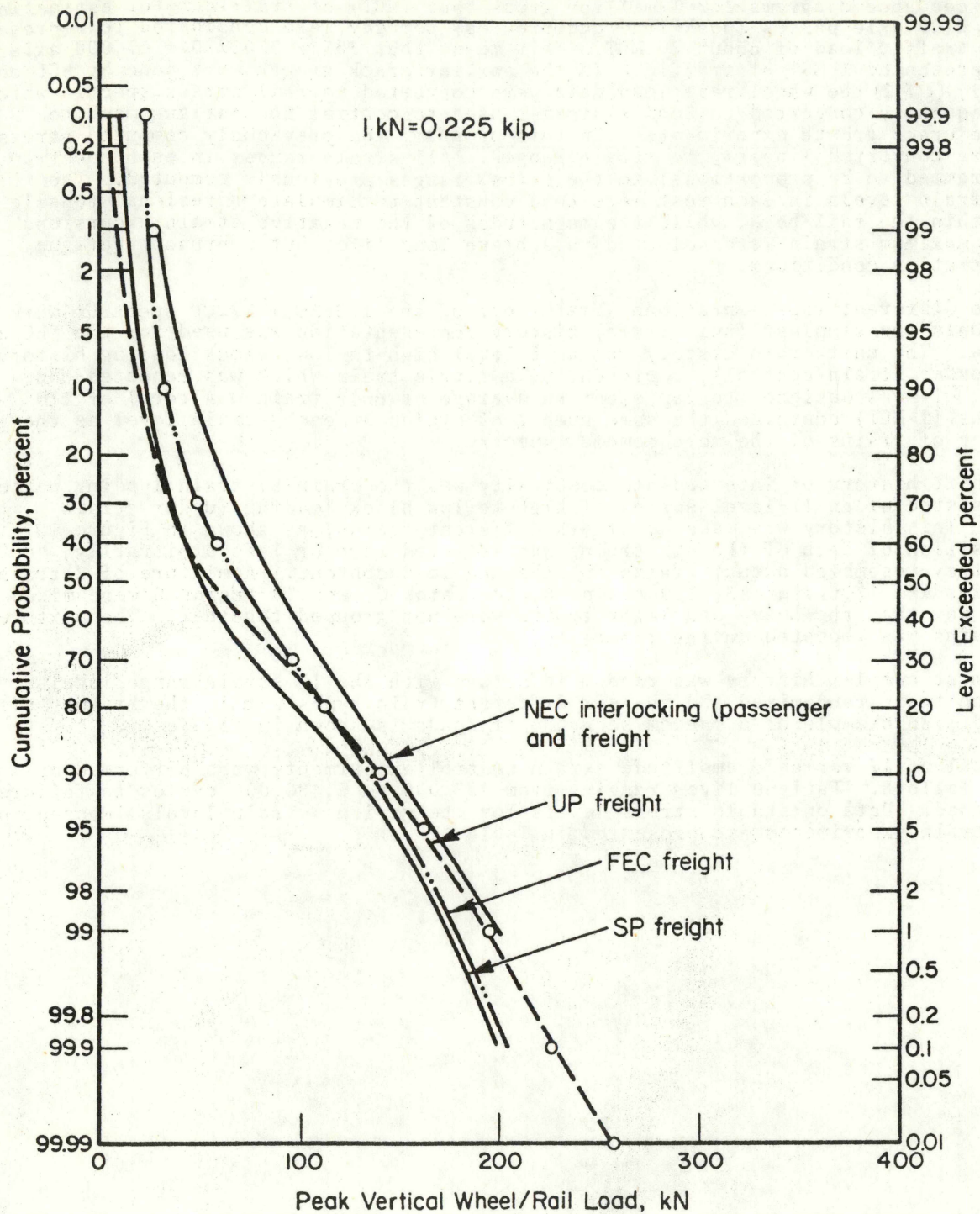


FIGURE 18. CUMULATIVE PROBABILITY PLOT OF PEAK VERTICAL WHEEL RAIL LOADS

spectrum used in this program was based on the NEC wheel rail loads, while the least severe was based on the SP wheel rail loads. The third spectrum used in this program was based on a combination of the UP and FEC wheel rail load distributions; it fell intermediate to the NEC and SP spectra.

Each of the three basic spectra was converted from cumulative probability curves to load exceedance diagrams for 1-million gross tons (MGT) of traffic. For estimating purposes, 3700 axle passes (peak load occurrences) per day were considered to represent an annual traffic load of about 20 MGT. This meant that $365 \times 3700/20 = 67,000$ axle passes represented 1 MGT of traffic. In the earlier crack growth work done by BCL on rail steel, (1 & 2) the wheel rail load data were converted to rail stress spectra which were subsequently converted to load histories used to control the fatigue machine during the crack growth experiments. In this program, the previously computed stress ranges were converted linearly to strain ranges. All strain ranges in each spectrum were programmed to be proportional to the stress ranges previously computed. The maximum strain levels in each test were held constant to simulate a residual tensile strain within the rail head, while the magnitudes of the negative strain excursions from that maximum strain were selected to achieve long life, but nonrunout fatigue crack initiation conditions.

Three different representations (histories) of the $1/2\text{FEC} + 1/2\text{UP}$ spectrum were tested. Only the simplest (unit train) history representation was used for the NEC and SP spectra. The unit train history was an 8-level high-to-low, block loading history (applied under strain control), representing a single train which was repeated continuously. It was designed to represent an average or unit train. A total of 170 unit trains (1 MGT) contained the same number of cycles at each strain level as the same number of trains of the more complex spectra.

The next history of intermediate complexity was the train-by-train loading pattern, which consisted of an 11-level series of high-to-low block loading (under strain control). This history was made up of six different trains, as shown in Figure 19. The composition of each of the six trains was selected more or less arbitrarily, however, they resembled actual trains in size and load content. A mixture of 2 trains A1, 6 trains A2, 12 trains A3, 120 trains B, 20 trains C, and 10 trains D were mixed in such a way that the heavy and light trains were not grouped together. The mixture of 170 trains was repeated during the tests.

The most complex history was random in nature with the 11 strain range levels within each train randomized and the six different train types within the history also randomized. An example of a random sequence of loads is shown in Figure 20.

A total of 17 variable amplitude strain control experiments were performed as listed in Table 8. Fatigue lives ranging from 127,000 to 6,480,000 cycles to failure were obtained. Data on stable stress levels for the various strain levels imposed in the unit train experiments are presented in Table 9.

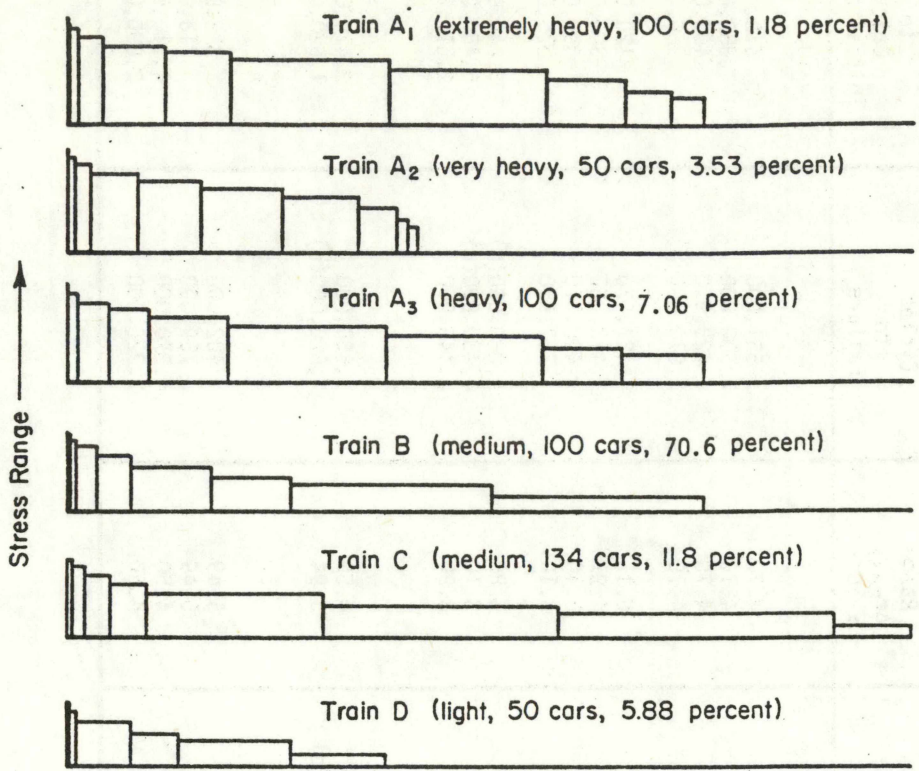


FIGURE 19. TRAIN COMPOSITIONS FOR TRAIN-BY-TRAIN AND RANDOM HISTORIES

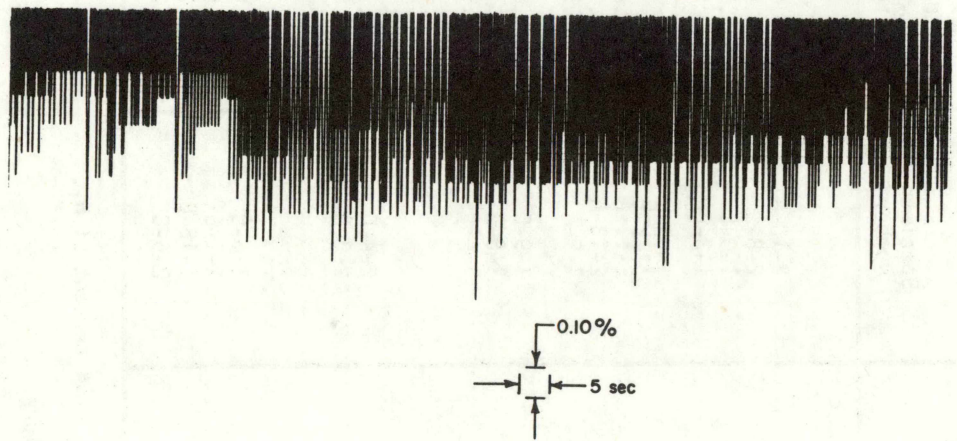


FIGURE 20. PART OF THE STRAIN HISTORY OF THE 11-LOAD RANDOM SERVICE SIMULATION EXPERIMENTS

TABLE 8. VARIABLE STRAIN AMPLITUDE FATIGUE TEST RESULTS

Spectrum Description	Specimen Number	Maximum Strain, ϵ_{\max} , x 10 ⁻³	Stable Maximum Stress, σ_{\max} , ksi	Maximum Strain Range $\Delta\epsilon_{\max}$, x 10 ⁻³	Cycles to Failure	Computed Cycles to Crack Initiation(a)
<u>Unit Train</u>						
½FEC + ½UP	2-10-A	3.90	60.3	4.70	551,000	518,000
	2-8-C	3.90	59.1	4.70	2,500,000	2,350,000
	1-3-C	2.50	52.4	4.70	428,910	403,000
	1-3-E	2.50	50.4	4.70	2,070,000	1,950,000
NEC	1-10-C	4.70	59.8	6.15	127,570	120,000
	2-11-A	3.80	59.2	4.97	413,360	389,000
	2-13-A	2.50	48.9	5.10	420,110	395,000
	1-9-A	2.50	51.8	5.10	717,650	675,000
SP	1-9-C	3.80	56.7	3.80	4,080,000(b)	3,840,000(b)
	1-8-A	3.10	59.5	3.10	6,480,000(c)	>6,480,000(c)
	1-4-C	2.50	55.9	3.90	2,140,000	2,010,000
<u>Train by Train</u>						
½FEC + ½UP	2-4-C	3.20	65.2	4.50	3,630,000	3,410,000
	2-8-A	2.80	- (d)	3.94	1,620,000(b)	1,520,000(b)
<u>Random</u>						
½FEC + ½UP	1-6-C	3.90	58.4	5.49	402,000	378,000
	2-1-E	3.90	59.6	5.49	759,000	713,000
	1-13-E	3.20	59.4	4.50	4,370,000	4,110,000
	2-6-C	3.20	63.3	4.50	2,220,000	2,090,000

(a) Based on $N_i = 94$ percent of N_f .

(b) Fillet failure.

(c) Did not fail, runout.

(d) Information not available.

TABLE 9. STABLE STRESS RESPONSE OF UNIT TRAIN TEST SPECIMENS

Spectrum Description	Specimen Identification	Maximum Stress, σ_{max} , ksi	1	2	Stress Level			6	7	8
					3	4	5			
					Minimum Stress, ksi					
$\frac{1}{2}$ FEC + $\frac{1}{2}$ UP	2-10-A	60.3	-48.1	-36.4	-30.8	-24.3	-14.3	-1.8	15.3	30.3
	2-8-C	59.1	-48.9	-36.7	-30.8	-23.2	-13.0	-1.6	15.3	30.0
		Avg. 59.7	-48.5	-36.5	-30.8	-23.6	-13.6	-1.7	15.3	30.1
	1-3-C	52.4	-55.0	-42.0	-37.4	-29.4	-20.1	-8.4	8.4	23.1
	1-3-E	50.4	-53.3	-40.1	-34.6	-27.3	-17.5	-7.3	8.5	22.2
		Avg. 51.4	-54.1	-41.0	-36.0	-28.3	-18.8	-7.8	8.4	22.7
NEC	1-10-C	59.8	-60.4	-49.1	-43.0	-37.9	-30.7	-20.4	-10.3	7.2
	2-11-A	59.2	-51.9	-38.6	-31.0	-24.4	-16.3	-4.5	5.3	19.2
	2-13-A	48.9	-54.2	-45.2	-38.6	-32.9	-25.5	-16.4	-7.4	6.6
	1-9-A	51.8	-56.4	-44.8	-37.0	-29.5	-21.6	-11.6	-2.1	12.0
		Avg. 50.4	-55.3	-45.0	-37.8	-31.2	-23.6	-13.0	-4.7	9.3
SP	1-9-C	56.7	-37.8	-33.3	-25.5	-17.2	-7.0	4.1	18.1	32.9
	1-4-C	55.9	-43.1	-38.0	-29.8	-21.3	-8.7	3.4	18.1	32.8
	1-8-A	59.5	-26.9	-22.4	-14.2	-6.2	4.1	14.4	26.7	39.1

5. DAMAGE ACCUMULATION MODEL

The development of a damage accumulation model for crack initiation that would be useful in the reliability analysis of railroad rails involved several interrelated tasks, including 1) the definition of an initiation crack size, 2) the statistical definition of the constant amplitude crack initiation data on new and used rail material, and 3) the development of a damage model which could be used to predict variable amplitude crack initiation fatigue performance from constant amplitude crack initiation data. These tasks are reviewed in the following sections.

5.1 DEFINITION OF INITIATION CRACK SIZE

It was shown earlier in Figure 9 that 85 to 95 percent of the total cycles to failure were involved in initiating a crack about 0.3-inch deep in the BCL specimen tested at $R = -1.0$. The work presented in this section was done to answer the following questions: (1) how is the transition crack size affected by stress ratio, and (2) at what initiation crack depth are stresses near the endurance limit sufficient to give crack tip stress intensities near the threshold for crack propagation? (Note that a crack initiated at a stress just above the endurance limit must be of sufficient size to be propagated at that same stress. Since the stress intensity depends on stress and crack size, the threshold stress intensity for crack growth can be exceeded only if the crack is large enough at a given stress.)

In reviewing past BCL work, (1) it is possible to determine that likely threshold stress intensity levels for rail steel at different stress ratios were as follows:

<u>Stress Ratio</u>	<u>Stress Intensity Range at Threshold ΔK, ksi-in.^{1/2}</u>
-1.0	14 - 18
0.10	12 - 16
0.50	7 - 9

In order to use this information effectively, it was necessary to know the relationship between crack depth and stress intensity for the test specimen being used in all fatigue tests. A recent publication by Dauod, et al, (16) shows that the effects of geometry on stress intensity are small (<3 percent) for crack depths less than 0.050-inch in the BCL and BCAC specimen of 0.250-inch diameter. In other words, the general formula for stress intensity could be used without a geometry factor as follows:

$$\Delta K = \Delta \sigma \sqrt{\pi a} , \text{ ksi-in.}^{1/2} \quad (5)$$

Where $\Delta \sigma$ = stress range, ksi

a = crack depth, inch

π = Pi (3.1416).

Using the above expression, it was possible to develop constant stress-intensity-range lines on a plot of maximum stress versus crack depth. These curves are shown in Figures 21 through 23 for the test stress ratios of -1.0, 0.1 and 0.5. The approximate endurance limits obtained from constant amplitude fatigue experiments are also indicated. The intersection of the threshold stress-intensity lines with the endurance limit band creates a zone of particular interest. It is within this zone that stresses near the endurance limit also cause stress intensities near the threshold for crack propagation. The crack depths associated with this zone are logically associated with the transition crack size between crack initiation and propagation. The relationship between transition crack size and stress ratio is shown in Figure 24. Obviously, the apparent equivalent initial flaw size decreases with increasing stress ratio. At an $R = -1.0$, a crack depth of 0.03-inch is representative, but crack depths as small as 0.006-inch are representative at an $R = 0.5$. The variable size of the transition flaw size shows its non-unique, empirical nature. It also illustrates

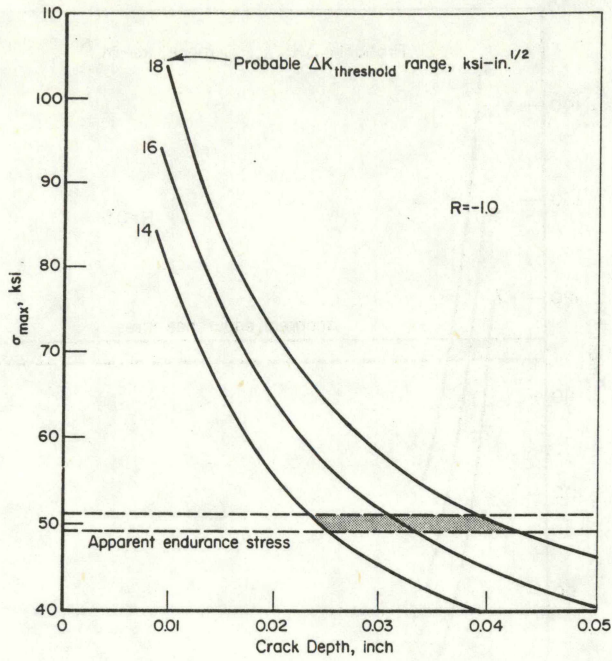


FIGURE 21. THRESHOLD VS. ENDURANCE LIMIT FOR $R = -1.0$

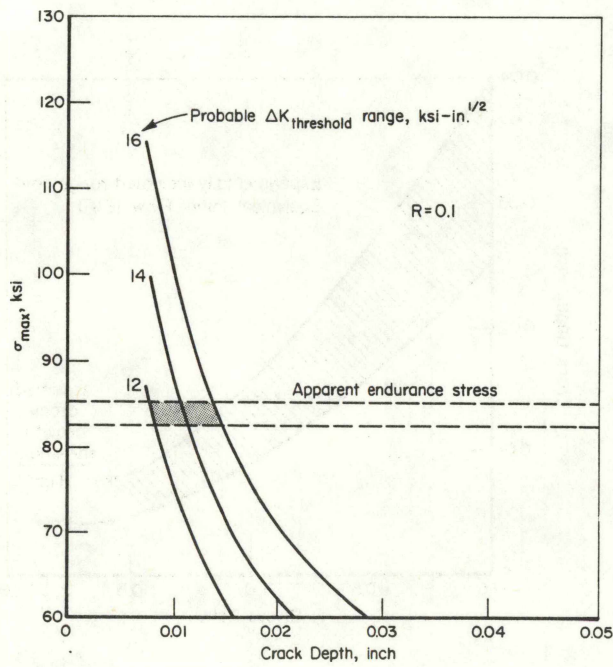


FIGURE 22. THRESHOLD VS. ENDURANCE LIMIT FOR $R = 0.10$

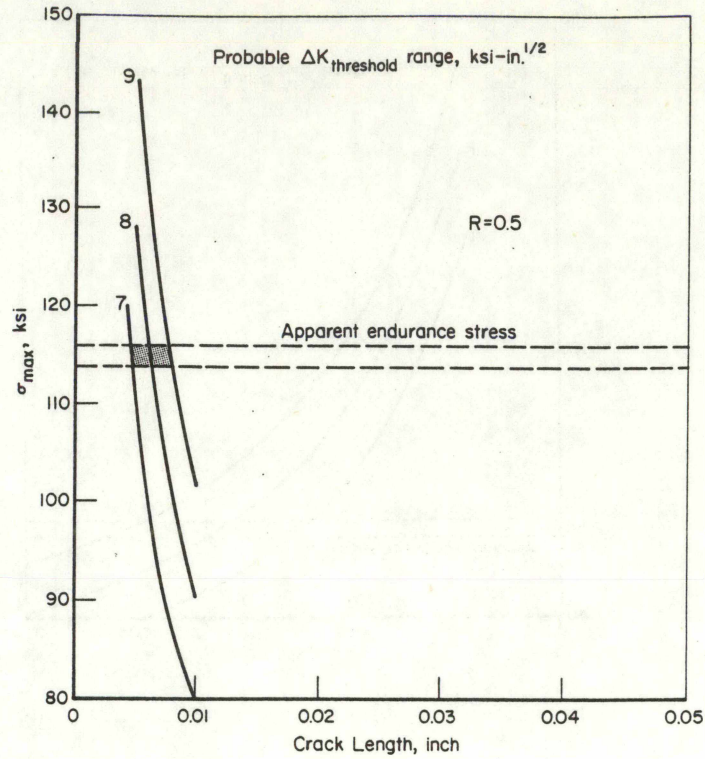


FIGURE 23. THRESHOLD VS. ENDURANCE LIMIT FOR R = 0.50

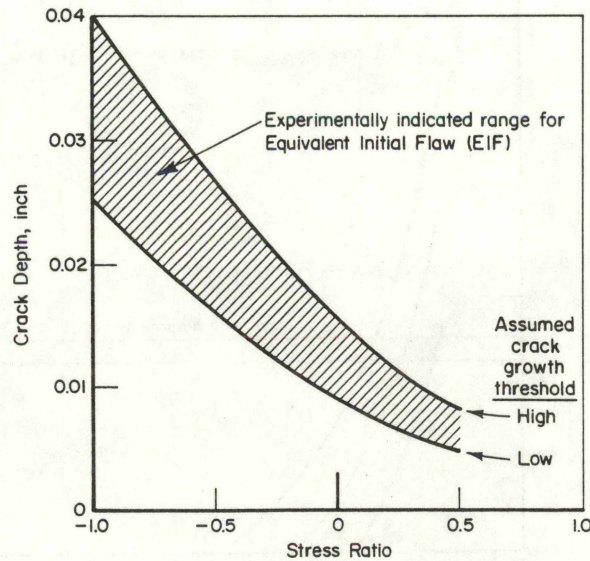


FIGURE 24. APPARENT OR EQUIVALENT INITIAL FLAW TRANSITION CRACK LENGTH (EIF) BETWEEN INITIATION AND PROPAGATION FOR RAIL STEEL FATIGUE SPECIMENS

the problem in the selection of a meaningful transition flaw size for a rail reliability analysis. A 0.03-inch flaw size was selected more or less arbitrarily, because crack propagation is expected at this crack size for all stress ratios above -1.0.

5.2 STATISTICAL DEFINITION OF CONSTANT AMPLITUDE FATIGUE DATA

The variability in fatigue data is of prime importance in a rail reliability analysis. For this reason, all of the unused and used rail crack initiation data were reviewed to provide a statistical definition of those data.

5.2.1 Unused Rail Crack Initiation Data

Through the use of the equivalent strain factor (Equation (1)), it was possible to combine all of the unused rail crack initiation data into a single fatigue curve, with the exception of those for transverse specimens. Grouped data of all the longitudinal orientations are shown in Figure 25. Some scatter is evident, but there is no consistent trend or layering of the data with either stress ratio or specimen location within the rail head. Two other things are also noted. First, the limited data for periodic overstrains shown also illustrate the dramatic effect of overstrains on high cycle fatigue performance. Second, the percent of runouts (shown for $\log \epsilon_{eq}$ value of -2.55 and below) indicates that the rate of increase in percent of runouts depends upon the stress ratio. These data are not conclusive but perhaps should be taken into account in reliability analyses involving constant amplitude fatigue data near the so-called endurance limit. The periodic overstrain data seem to indicate that the endurance limit found in the constant amplitude tests may not apply for variable amplitude loading conditions.

In order to assess the variability of the data for different life ranges, the data were subdivided into four groups as follows:

Group	Equivalent Strain
1	$\epsilon_{eq} < 4.40 \times 10^{-3}$
2	$3.20 \times 10^{-3} \leq \epsilon_{eq} < 3.60 \times 10^{-3}$
3	$3.00 \times 10^{-3} \leq \epsilon_{eq} < 3.20 \times 10^{-3}$
4	$2.80 \times 10^{-3} \leq \epsilon_{eq} < 3.00 \times 10^{-3}$

Most tests completed below an ϵ_{eq} of 2.80×10^{-3} were runouts and were therefore not included in this analysis.

The data within each group were ranked and the statistical parameters shown in Table 10 were calculated. These statistics include an average life $10 \log N_i$, a coefficient of variation, median ranks (for plotting on log-normal paper) and fraction failed (for plotting on Weibull paper). The average life, of course, goes up with decreasing equivalent strain. The coefficient of variation also increases somewhat with increasing life which has been noted elsewhere with some steel alloys. This increase in scatter is evident in Figure 26 where the four groups of data are displayed on log-normal probability paper. The increase in slope of the data trends with increasing crack initiation life indicates increased variability. Several observations can be made here. First, in the area of principal interest (early failures in the long life regime) the distribution of failures follows a log-normal trend reasonably well. Second, the breakpoint in the curve for the longest life test series seems to be indicative of a transition in the failure mechanism. It is at least plausible that the early failures preceding the transition are representative of specimens already containing microcracks, and the late failures (and runouts) following the transition are representative of essentially defect-free rail specimens. Whatever the explanation, the area of prime interest involving early failures follows log-normal trends.

The data were also plotted on two-parameter Weibull paper as shown in Figure 27. At the shorter lives (Groups 1 and 2), there are too few data to verify trends, but for Groups 3 and 4, the data fairly clearly do not follow a two-parameter Weibull, unless one resorts to a two or three piece linear representation of the data.

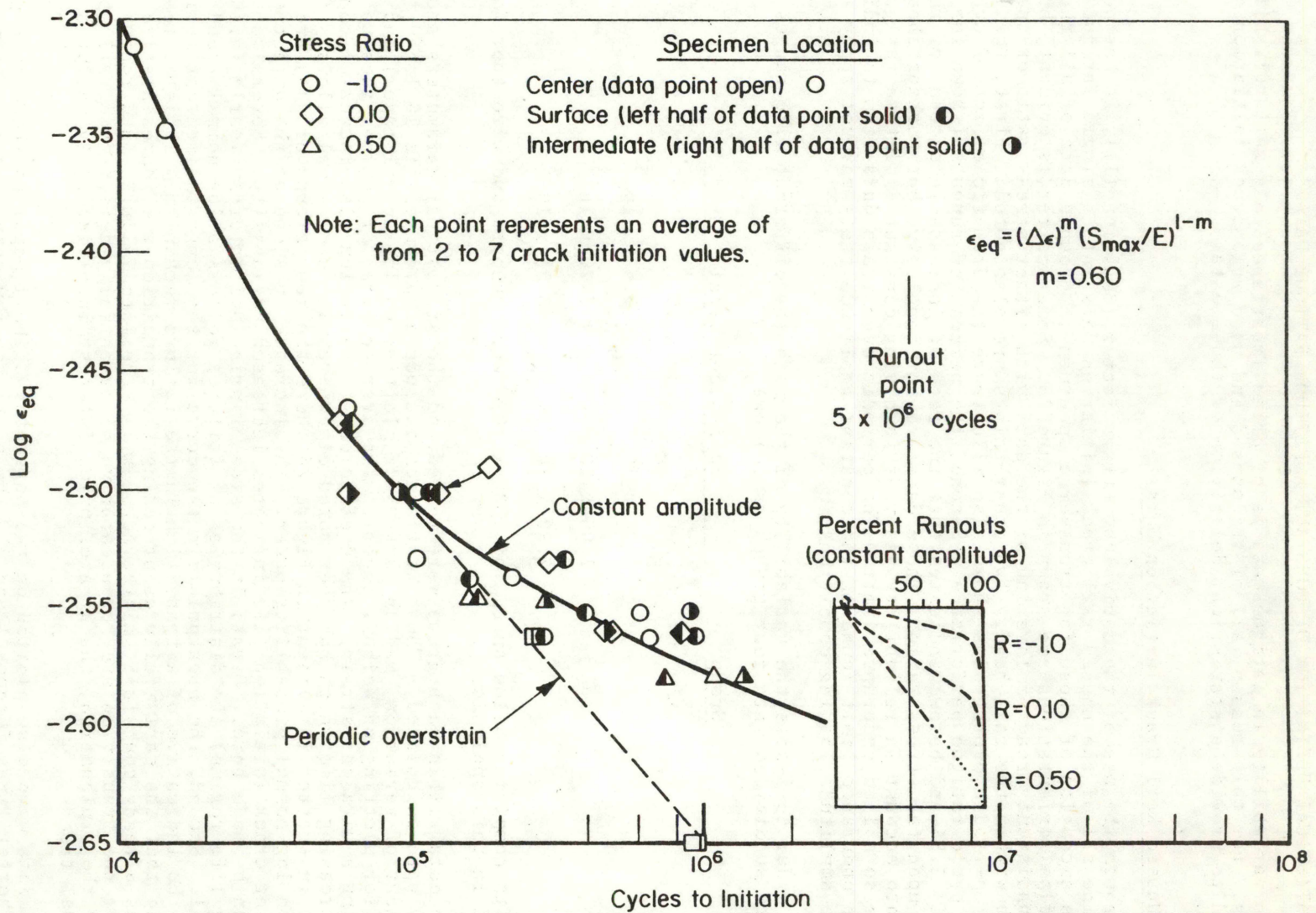


FIGURE 25. FATIGUE LIFE TRENDS FOR GROUPED DATA VS. EQUIVALENT STRAIN

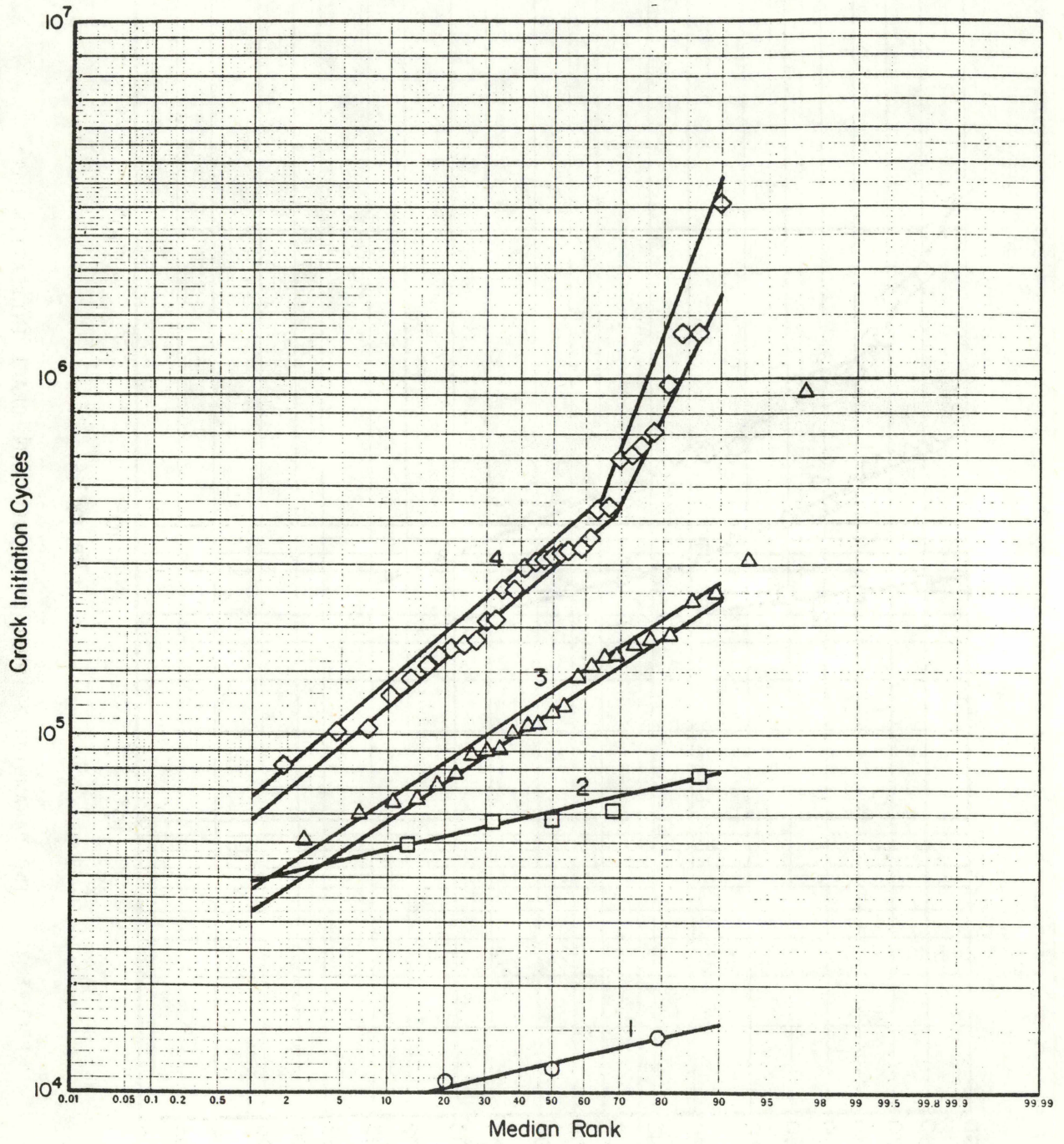


FIGURE 26. LOG NORMAL PROBABILITY PLOT OF UNUSED RAIL CRACK INITIATION DATA

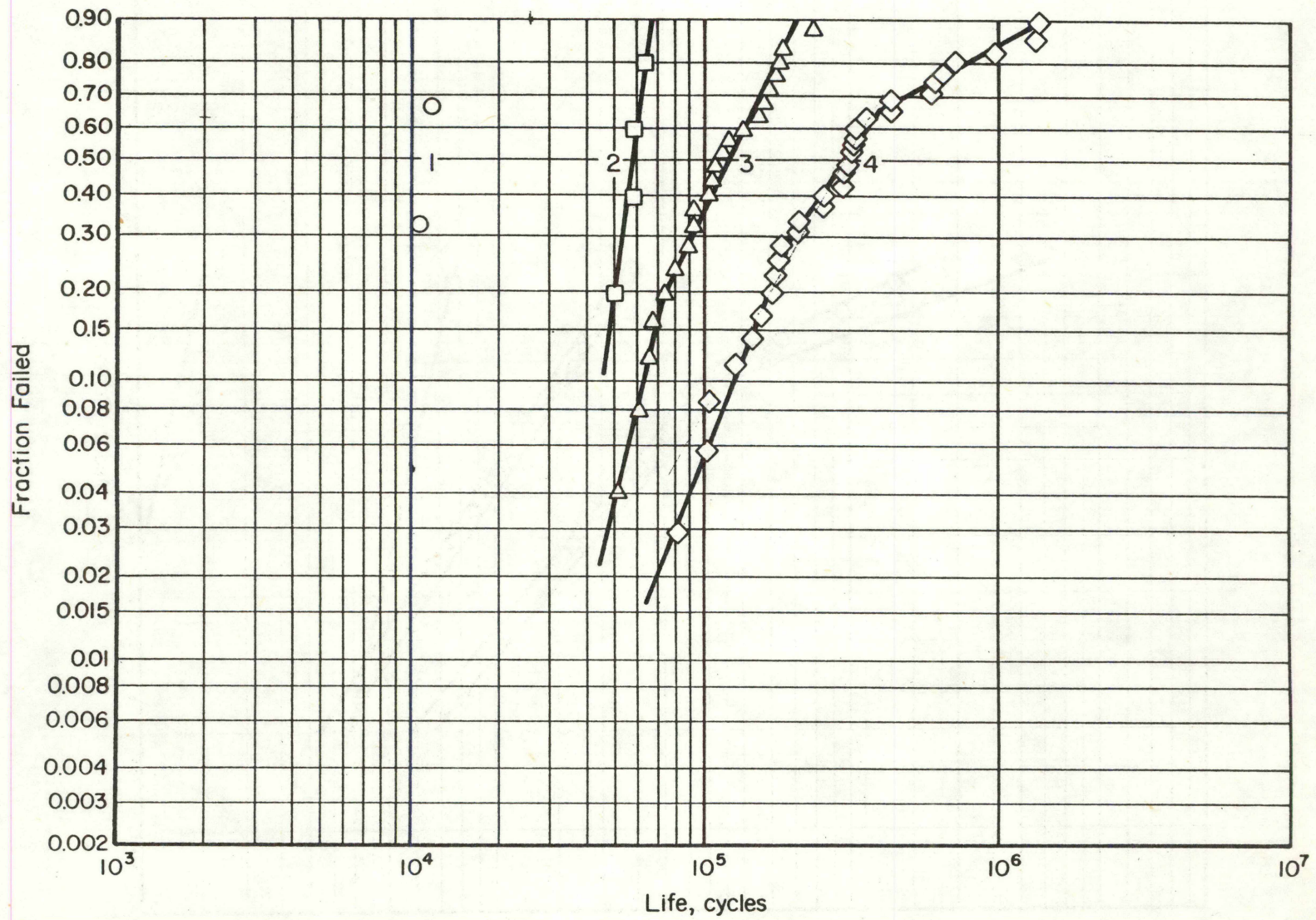


FIGURE 27. TWO-PARAMETER WEIBULL OF UNUSED RAIL CRACK INITIATION DATA

TABLE 10. GROUPED AND RANKED CRACK INITIATION DATA ON UNUSED RAIL MATERIAL

GROUP	RANK	FATIGUE LIFE	AVERAGE LIFE (LOG)	COEFFICIENT OF VARIATION, %	MEDIAN RANK	FRACTION FAILED
1	1	10775	12203	1.5	0.2063	0.33
	2	11770			0.5000	0.67
	3	14330			0.7937	1.00
2	1	49710	60133	1.5	0.1294	0.2
	2	57000			0.3147	0.4
	3	57610			0.5000	0.6
	4	62000			0.6853	0.8
	5	77690			0.8706	1.0
3	1	51000	128653	5.3	0.0277	0.04
	2	60000			0.0670	0.08
	3	65000			0.1064	0.12
	4	66000			0.1457	0.16
	5	72000			0.1851	0.20
	6	79000			0.2245	0.24
	7	88000			0.2638	0.28
	8	91000			0.3032	0.32
	9	92580			0.3425	0.36
	10	102000			0.3819	0.40
	11	107000			0.4212	0.44
	12	107000			0.4606	0.48
	13	115000			0.5000	0.52
	14	120000			0.5393	0.56
	15	144000			0.5787	0.60
	16	154000			0.6180	0.64
	17	163800			0.6574	0.68
	18	167000			0.6967	0.72
	19	177000			0.7361	0.76
	20	183300			0.7754	0.80
	21	187800			0.8148	0.84
	22	234700			0.8542	0.88
	23	246800			0.8935	0.92
	24	308000			0.9329	0.96
	25	924600			0.9722	1.00
4	1	81000	317924	6.5	0.0198	0.029
	2	102000			0.0480	0.057
	3	104000			0.0763	0.086
	4	127870			0.1043	0.114
	5	143000			0.1327	0.143
	6	157000			0.1610	0.171
	7	167000			0.1892	0.200
	8	173940			0.2175	0.229
	9	179290			0.2457	0.257
	10	183000			0.2740	0.286
	11	209000			0.3022	0.314
	12	210000			0.3305	0.343
	13	254000			0.3587	0.371
	14	256000			0.3870	0.400
	15	294000			0.4152	0.429
	16	303000			0.4435	0.457
	17	309000			0.4717	0.486
	18	315000			0.5000	0.514
	19	326000			0.5282	0.543
	20	328000			0.5564	0.571
	21	334000			0.5847	0.600
	22	358000			0.6129	0.629
	23	431000			0.6412	0.657

TABLE 10. (Concluded)

GROUP	RANK	FATIGUE LIFE	AVERAGE LIFE (LOG)	COEFFICIENT OF variation, %	MEDIAN RANK	FRACTION FAILED
	24	438000			0.6694	0.686
	25	589000			0.6977	0.714
	26	610000			0.7259	0.743
	27	645000			0.7542	0.771
	28	712000			0.7824	0.800
	29	973000			0.8107	0.829
	30	1314000			0.8389	0.857
	31	1324000			0.8672	0.886
	32	3026000			0.8954	0.914
	33	5080000R			0.9237	0.943
	34	5087000R			0.9519	0.971
	35	5100000R			0.9801	1.000

In summary, it appears that a log-normal or a two-parameter Weibull representation of the early failure data is useful only if the late failure nonlinearities can be ignored. This may well be the most reasonable approach, especially in view of the lack of ready alternatives. An assumption of homoscedasticity is also questionable, if such an assumption is used, it should be based on the slope of the low equivalent strain data groups in the early failure region (see Figure 26, data groups 3 and 4 below about a 60 percent median rank).

5.2.2 USED RAIL CRACK INITIATION DATA

Most of the used rail initiation data were generated at maximum stress levels of 85 and 95 ksi ($R = 0.10$). At the other three stress levels (of 105, 75, and 65 ksi), data on only one or two of the four used rail materials were generated — the fatigue lives obtained at these levels were, therefore, not representative of the overall collection of used rail materials and were omitted from this analysis.

The data generated at the two primary stress levels were ranked for statistical analysis in the manner shown in Table 11. The ranked data were plotted on normal probability paper in Figure 28 to evaluate their trends. Distinctly nonlinear patterns are evident at both stress levels. Since this result was considered unsatisfactory, the data were examined jointly, in an effort to better represent overall used rail fatigue data trends. Figure 29 shows the result of the data combination. A very nearly linear pattern is evident. The average fatigue life of this combined group was 147,900 with a coefficient of variation of 10.0.

The combined used rail fatigue data display mean fatigue life is nearly equal to the unused rail data (at $\log \epsilon_{eq} = -2.53$ $\bar{N}_i = 147,900$ for used rail, 180,000 for unused rail). The coefficient of variation of 10.0 for the used rail data is nearly double that found for unused rail material, however, and should be taken into account in the reliability analysis.

5.3 VARIABLE STRAIN AMPLITUDE CRACK INITIATION PREDICTION

Three different methods of predicting fatigue lives for the variable strain amplitude experiments were attempted. The basic element in each calculation was the equivalent strain factor, previously presented in Equation (1). Since strain was controlled in these spectrum tests, the various levels of strain range, $\Delta\epsilon$, were known and the maximum stable stress, σ_{max} , was necessarily measured or calculated. Where σ_{max} was computed, the cyclic stress-strain curve for the material was used.

Damage calculations for the three-unit train spectra are shown in Tables 12 through 14. Similar calculations for the train-by-train and random spectra are shown in Table 15. The individual methods of linear damage calculations involved the following variables:

<u>Method</u>	<u>Fatigue Curve</u>	<u>Maximum Stress</u>
1	Constant Amplitude	Actual
2	Periodic Overstrain	Actual
3	Periodic Overstrain	Computed

The results of these three damage calculations for all the spectra are summarized in Table 16. The results are presented graphically in Figures 30, 31, and 32 for Methods 1, 2, and 3, respectively. It is evident in Figure 30 that Method 1 overestimated actual crack initiation lives in nearly every case, in an unconservative manner. In Figure 31, it is evident that Method 2 provides a substantially improved prediction of actual crack initiation lives. For reference purposes, 1 and 2 standard deviation lines are constructed (based on a constant coefficient of variation of 5 percent). All data are contained within two standard deviations.

TABLE 11. GROUPED AND RANKED CRACK INITIATION DATA ON USED RAIL MATERIAL

MAXIMUM STRESS LEVEL, ESTIMATED STRAIN RANGE AND EQUIVALENT STRAIN	RANK	FATIGUE LIFE	AVERAGE LIFE	COEFFICIENT OF VARIATION, PERCENT	MEDIAN RANK	FRACTION FAILED
85 ksi $\Delta\epsilon = 2.75 \times 10^{-3}$ $\epsilon_{eq} = 2.75 \times 10^{-3}$ $\log \epsilon_{eq} = - 2.56$	1	45	173,400	9.6	0.033	0.048
	2	46			0.080	0.095
	3	53			0.126	0.143
	4	62			0.173	0.190
	5	83			0.220	0.238
	6	99			0.226	0.286
	7	121			0.313	0.333
	8	124			0.360	0.381
	9	124			0.407	0.429
	10	149			0.453	0.476
	11	180			0.500	0.524
	12	183			0.547	0.571
	13	359			0.593	0.619
	14	379			0.640	0.667
	15	495			0.687	0.714
	16	1064			0.733	0.762
	17	3170			0.780	0.810
	18-21	5000R				
95 ksi $\Delta\epsilon = 0.308$ $\epsilon_{eq} = 3.16 \times 10^{-3}$ $\log \epsilon_{eq} = - 2.50$	1	10	121,900	10.6	0.048	0.071
	2,3	23,29			0.118-0.0187	0.143-0.214
	4	64			0.257	0.286
	5	69			0.326	0.357
	6	97			0.396	0.429
	7	139			0.465	0.500
	8	199			0.535	0.571
	9	212			0.604	0.643
	10	267			0.674	0.714
	11	278			0.743	0.786
	12	375			0.813	0.857
	13	502			0.882	0.929
	14	689			0.952	1.00

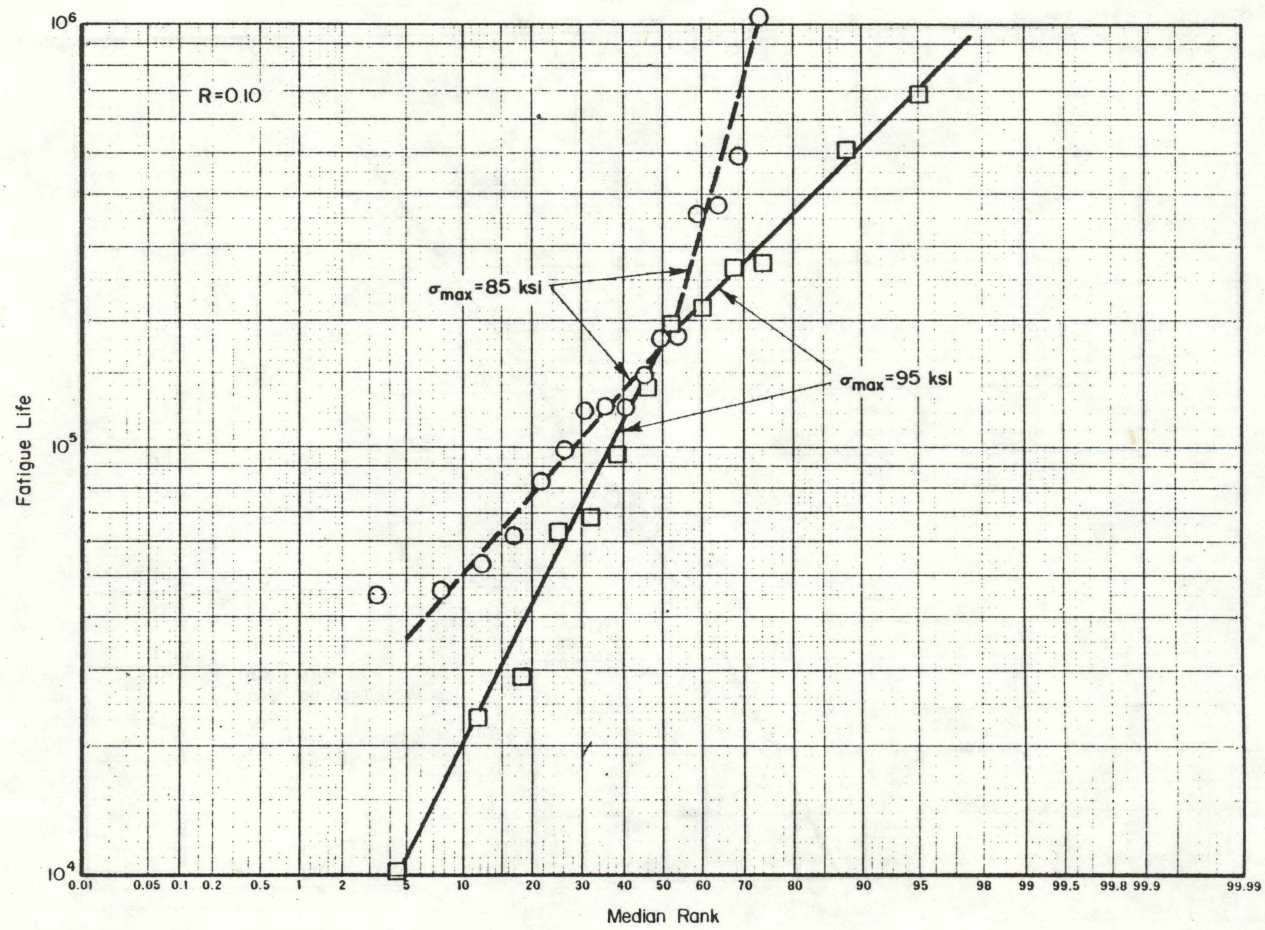


FIGURE 28. USED RAIL DATA, STRESS LEVELS COMBINED

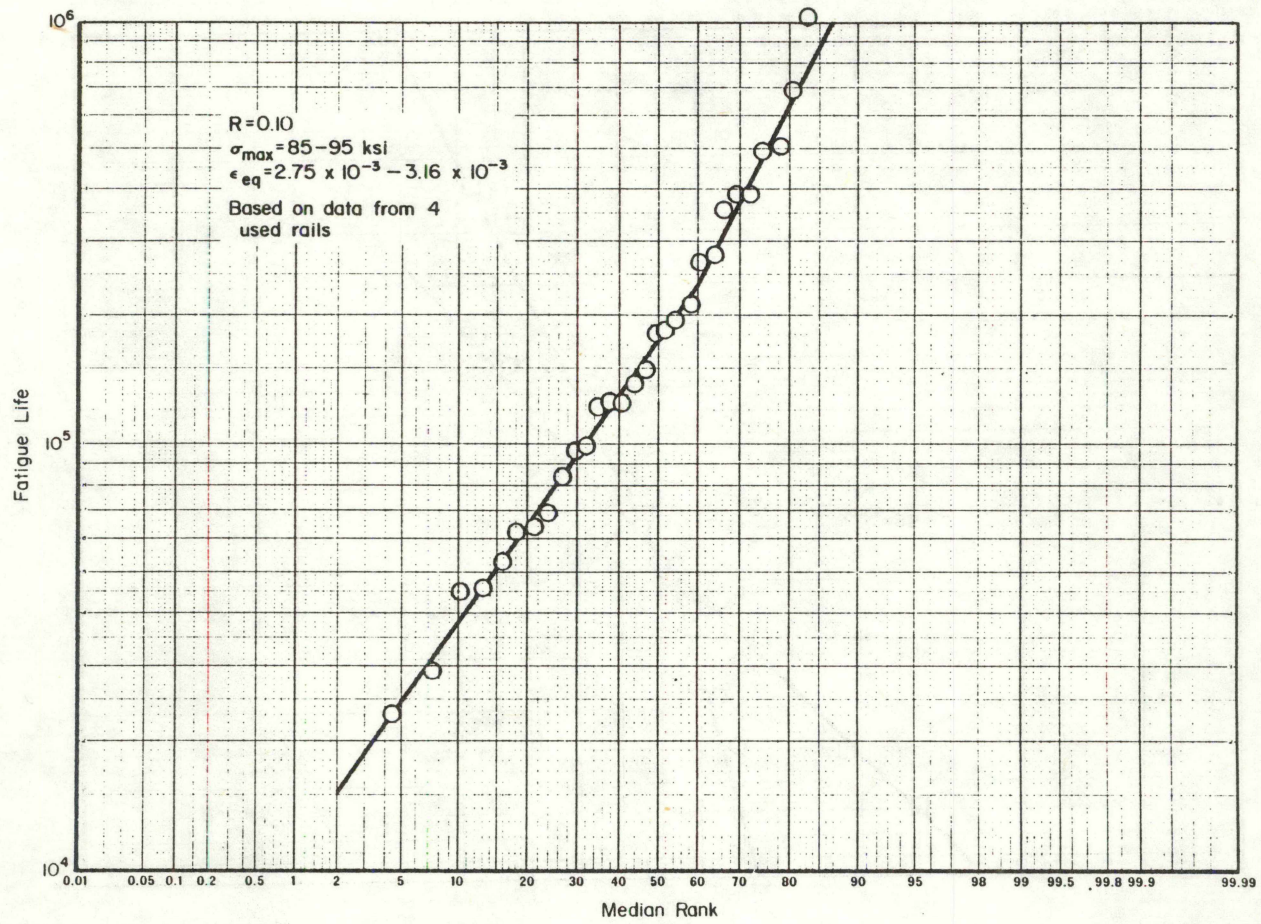


FIGURE 29. USED RAIL DATA, STRESS LEVELS PLOTTED SEPARATELY

TABLE 12. ONE-HALF FEC PLUS ONE-HALF UP UNIT TRAIN FATIGUE DAMAGE CALCULATIONS

SPECIMEN NUMBER	MAXIMUM STRAIN, $\epsilon_{\max} \times 10^{-3}$	STRAIN RANGE, $\Delta\epsilon \times 10^{-3}$	STABLE MAXIMUM STRESS, σ_{\max} ksi	STABLE STRESS RANGE, $\Delta\sigma$, ski	CYCLE PER BLOCKS, C_i	EQUIVALENT STRAIN $\epsilon_{eq}^{(a)} \times 10^{-3}$	METHOD 1	METHOD 2	METHOD 3	
							DAMAGE INCREMENT (b) $D_i \times 10^{-5}$	DAMAGE INCREMENT (c) $D_i \times 10^{-5}$	DAMAGE INCREMENT (c,d) $D_i \times 10^{-5}$	
2-10-A 2-8-C	3.90	4.71	59.7	108.2	1	3.48	2.21	2.17	3.26	
		3.92		96.2	5	3.12	4.81	5.05	7.63	
		3.61		90.5	6	2.97	3.26	4.29	6.48	
		3.22		83.3	18	2.77	3.54	7.91	12.00	
		2.75		73.3	30	2.52	1.16	6.81	10.47	
		2.28		61.4	60	2.25	0.29	6.16	9.40	
		1.65		44.4	60	1.85	0.01	1.57	2.44	
		1.10		29.6	120	1.45	----	0.57	0.87	
								15.28	34.53	52.55
								$N_f=1.96 \times 10^6$	$N_f=8.69 \times 10^5$	$N_f=5.71 \times 10^5$
1-3-C 1-3-E	2.50	4.71	51.4	105.5	1	3.28	1.50	1.43	1.59	
		3.92		92.4	5	2.94	2.38	3.33	3.66	
		3.61		87.4	6	2.79	1.32	2.77	3.14	
		3.22		79.7	18	2.61	1.30	5.22	5.80	
		2.75		70.2	30	2.37	0.38	4.43	4.98	
		2.28		59.2	60	2.12	0.10	4.07	4.63	
		1.65		43.0	60	1.75	----	1.06	1.20	
		1.10		28.7	120	1.37	----	0.38	0.43	
								6.98	22.69	25.43
								$N_f=4.30 \times 10^6$	$N_f=1.32 \times 10^6$	$N_f=1.18 \times 10^6$

(a) $\epsilon_{eq} = (\Delta\epsilon)^m (\sigma_{\max}/E)^{1-m}$, $m = 0.60$; $E = 29.0 \times 10^3$ ksi.

(b) $D_i = C_i/N_i$ where $N_i = 2.249 \times 10^{-5} \epsilon_{eq}^{-3.76} + 4.365 \times 10^{-43} \epsilon_{eq}^{-18.76}$.

(c) $D_i = C_i/N_i$ where $N_i = 3.02 \times 10^{-13} \epsilon_{eq}^{-6.99}$.

(d) σ_{\max} is computed from cyclic σ - ϵ curve.

TABLE 13. NEC UNIT TRAIN FATIGUE DAMAGE CALCULATIONS

SPECIMEN	MAXIMUM STRAIN, $\epsilon_{\max} \times 10^{-3}$	STRAIN RANGE, $\Delta\epsilon \times 10^{-3}$	MAXIMUM STABLE STRESS, σ_{\max} , ksi	STABLE STRESS RANGE, $\Delta\sigma$, ksi	CYCLES PER BLOCK,	EQUIVALENT STRAIN, ϵ_{eq} $\times 10^{-3}$	METHOD 1	METHOD 2	METHOD 3
							DAMAGE (b) INCREMENT $D_i \times 10^{-5}$	DAMAGE (c) INCREMENT $D_i \times 10^{-5}$	DAMAGE (c,d) INCREMENT ¹ $D_i \times 10^{-5}$
1-10-C	4.70	6.15	59.8	120.2	1	4.09	4.60	13.21	7.20
		5.11		108.9	5	3.66	14.35	15.41	24.97
		4.54		102.8	6	3.41	11.77	11.27	22.74
		4.07		97.7	18	3.19	21.40	21.22	43.07
		3.60		90.5	30	2.96	15.60	20.96	42.96
		3.03		80.2	60	2.67	6.41	20.39	41.93
		2.56		70.1	60	2.42	1.11	10.26	20.93
		1.90		52.6	120	2.02	0.08	5.80	11.95
							75.32	118.5	215.75
							$N_f=3.98 \times 10^5$	$N_f=2.53 \times 10^5$	$N_f=1.39 \times 10^5$
2-11-A	3.80	4.97	59.2	111.7	1	3.58	2.58	2.64	3.93
		4.13		98.4	5	3.21	6.28	6.16	9.02
		3.67		90.8	6	2.99	3.55	4.50	6.62
		3.29		84.2	18	2.80	4.19	8.53	12.58
		2.91		76.1	30	2.60	2.02	8.47	12.53
		2.45		64.3	60	2.34	0.60	8.11	12.17
		2.07		54.5	60	2.12	0.10	4.07	5.98
		1.54		40.6	120	1.77	0.01	2.30	3.51
							19.33	44.78	66.34
							$N_f=1.55 \times 10^6$	$N_f=6.70 \times 10^5$	$N_f=4.52 \times 10^5$
2-13-A 1-9-A	2.50	5.10	50.4	105.7	1	3.41	1.96	3.92	2.21
		4.24		95.4	5	3.05	3.76	4.31	5.16
		3.77		88.2	6	2.85	1.83	3.22	3.72
		3.38		81.6	18	2.67	1.92	6.12	7.15
		2.99		74.0	30	2.48	0.87	6.09	7.19
		2.51		63.4	60	2.23	0.25	5.79	6.76
		2.12		55.1	60	2.01	0.04	2.80	3.33
		1.58		41.1	120	1.69	----	1.67	1.96
							10.63	33.92	37.48

(a) $\epsilon_{\text{eq}} = (\Delta\epsilon)^m (\sigma_{\max}/E)^{1-m}$, $m = 0.60$; $E = 29.0 \times 10^3$ ksi.

(b) $D_i = C_i/N_i$ where $N_i = 2.249 \times 10^{-5} \epsilon_{\text{eq}}^{-3.76} + 4.365 \times 10^{-43} \epsilon_{\text{eq}}^{-18.76}$.

(c) $D_i = C_i/N_i$ where $N_i = 3.02 \times 10^{-13} \epsilon_{\text{eq}}^{-6.99}$.

(d) σ_{\max} is computer from cyclic σ - ϵ curve.

TABLE 14. SP UNIT TRAIN FATIGUE DAMAGE CALCULATIONS

SPECIMEN	MAXIMUM STRAIN, $\epsilon_{\max} \times 10^{-3}$	STRAIN RANGE, $\Delta\epsilon \times 10^{-3}$	MAXIMUM STABLE STRESS, σ_{\max} ksi	STABLE STRESS RANGE, $\Delta\sigma$ ksi	CYCLE PER BLOCK	EQUIVALENT STRAIN, (a) $\epsilon_{\text{eq}} \times 10^{-3}$	METHOD 1	METHOD 2	METHOD 3
							DAMAGE (b) INCREMENT $D_i \times 10^{-5}$	(DAMAGE (c) INCREMENT $D_i \times 10^{-5}$	DAMAGE (c,d) INCREMENT $D_i \times 10^{-5}$
1-9-C	3.80	3.82	56.7	94.5	1	3.01	0.28	0.79	1.31
		3.59		90.0	5	2.90	1.97	3.03	5.05
		3.21		82.2	6	2.71	0.82	2.26	3.81
		2.83		73.9	18	2.51	0.65	3.97	6.62
		2.37		63.7	30	2.26	0.16	3.18	5.28
		1.92		52.6	60	1.99	0.03	2.61	4.34
		1.38		38.6	60	1.63	----	0.65	1.11
		0.84		23.8	120	1.21	----	0.16	0.27
						3.91	16.65	27.79	
						$N_f=7.67 \times 10^6$	$N_f=1.80 \times 10^6$	$N_f=1.08 \times 10^6$	
1-8-A	3.10	3.12	59.5	86.4	1	2.71	0.14	0.38	0.40
		2.93		81.9	5	2.61	0.36	1.45	1.53
		2.62		73.7	6	2.44	0.13	1.09	1.15
		2.31		65.7	18	2.27	0.10	1.97	2.03
		1.93		55.4	30	2.04	0.02	1.55	1.61
		1.56		45.1	60	1.79	----	1.25	1.30
		1.13		32.8	60	1.48	----	0.33	0.35
		0.69		20.4	120	1.10	----	0.08	0.09
						0.75	8.09	8.46	
						$N_f=3.97 \times 10^7$	$N_f=3.71 \times 10^6$	$N_f=3.55 \times 10^6$	
1-4-C	2.50	3.82	55.9	99.0	1	2.99	0.59	0.75	0.67
		3.59		93.9	5	2.88	1.78	2.88	2.55
		3.21		85.7	6	2.69	0.73	2.15	1.94
		2.83		77.2	18	2.50	0.60	3.86	3.35
		2.37		64.6	30	2.25	0.14	3.08	2.72
		1.92		52.5	60	1.98	0.03	2.52	2.19
		1.38		37.8	60	1.62	----	0.62	0.54
		0.84		23.1	120	1.20	----	0.15	0.13
						3.87	16.01	14.09	
						$N_f=7.74 \times 10^6$	$N_f=1.87 \times 10^6$	$N_f=2.13 \times 10^6$	

(a) $\epsilon_{\text{eq}} = (\Delta\epsilon)^m (\sigma_{\max}/E)^{1-m}$, $m = 0.60$; $E = 29.0 \times 10^3$ ksi.

(b) $D_i = C_i/N_i$ where $N_i = 2.249 \times 10^{-5} \epsilon_{\text{eq}}^{-3.76} + 4.365 \times 10^{-43} \epsilon_{\text{eq}}^{-18.76}$.

(c) $D_i = C_i/N_i$ where $N_i = 3.02 \times 10^{-13} \epsilon_{\text{eq}}^{-6.99}$.

(d) σ_{\max} is computed from cyclic σ - ϵ curve.

TABLE 15. FATIGUE DAMAGE CALCULATIONS FOR RANDOM AND TRAIN-BY-TRAIN SPECTRA (METHOD 3)

SPECIMEN IDENTIFICATION	MAXIMUM STRAIN, $\epsilon_{\max} \times 10^{-3}$	STABLE MAXIMUM STRESS, σ_{\max} (a)	STRAIN RANGE MULTIPLIER	STRAIN RANGE, $\Delta\epsilon \times 10^{-3}$	EQUIVALENT STRAIN, $\epsilon_{\text{eq}} \times 10^{-3}$ (b)	CYCLE PER MGT, C_i	DAMAGE INCREMENTS (c) D_i	
1-6-C and 2-1-E	3.9	68.9	1.407	5.49	4.04	2	0.10×10^{-3}	
			1.320	5.15	3.88	8	0.35×10^{-3}	
			1.223	4.77	3.71	40	1.36×10^{-3}	
			1.127	4.40	3.54	150	3.66×10^{-3}	
			1.055	4.11	3.40	800	14.73×10^{-3}	
			0.922	3.60	3.14	1000	10.56×10^{-3}	
			0.825	3.22	2.93	3000	19.52×10^{-3}	
			0.703	2.74	2.66	5000	16.55×10^{-3}	
			0.563	2.20	2.33	10,000	13.12×10^{-3}	
			0.422	1.65	1.96	10,000	3.92×10^{-3}	
			0.290	1.13	1.57	20,000	1.66×10^{-3}	
								$\Sigma 85.53 \times 10^{-3}$
			1-13-E, 2-6-C and 2-4-C	3.2	61.7	1.407	4.50	3.43
1.320	4.22	3.30				8	12.0×10^{-5}	
1.223	3.91	3.15				40	43.2×10^{-5}	
1.127	3.61	3.01				150	117.8×10^{-5}	
1.055	3.38	2.89				800	472.9×10^{-5}	
0.922	2.95	2.66				1000	331.1×10^{-5}	
0.825	2.64	2.49				3000	626.0×10^{-5}	
0.703	2.25	2.26				5000	529.9×10^{-5}	
0.563	1.80	1.98				10,000	420.4×10^{-5}	
0.422	1.35	1.67				10,000	127.9×10^{-5}	
0.290	0.93	1.33				20,000	52.1×10^{-5}	
								$\Sigma 2735.3 \times 10^{-5}$
2-8-A	2.8	57.1				1.407	3.94	3.07
			1.320	3.70	2.96	8	5.59×10^{-5}	
			1.223	3.42	2.82	40	19.92×10^{-5}	
			1.127	3.16	2.69	150	53.71×10^{-5}	
			1.055	2.95	2.58	800	213.95×10^{-5}	
			0.922	2.58	2.38	1000	152.15×10^{-5}	
			0.825	2.31	2.23	3000	289.58×10^{-5}	
			0.703	1.97	2.03	5000	250.24×10^{-5}	
			0.563	1.58	1.78	10,000	199.72×10^{-5}	
			0.422	1.18	1.49	10,000	57.62×10^{-5}	
			0.290	0.81	1.19	20,000	23.94×10^{-5}	
								$\Sigma 1268.22 \times 10^{-5}$

(a) $\sigma_{\max} = 1.758 \times 10^3 \epsilon_a^{0.583}$ for $\epsilon_a = \epsilon_{\max} \geq 1.344 \times 10^{-3}$.

(b) $\epsilon_{\text{eq}} = (\Delta\epsilon)^m (\sigma_{\max}/E)^{1-m}$ where $m = 0.60$, $E = 27.0 \times 10^6$.

(c) $D_i = C_i/N_i$ where $C_i = 3.090 \times 10^{-4} \epsilon_{\text{eq}}^{-3.265}$ for $\epsilon_{\text{eq}} > 3.802 \times 10^{-3}$.

TABLE 16. ESTIMATED AND ACTUAL SPECIMEN CYCLES TO FAILURE FOR VARIABLE AMPLITUDE TESTS

SPECTRUM DESCRIPTION	SPECIMEN NUMBER	N_i , BASED ON CONSTANT AMPLITUDE CURVE AND ACTUAL, σ_{max}	N_i , BASED ON PERIODIC OVERSTRAINS CURVE AND ACTUAL, σ_{max}	N_i , BASED ON PERIODIC OVERSTRAIN CURVE AND CALCULATED, σ_{max}	N_i , ACTUAL (a)
Unit Train $\frac{1}{2}$ FEC + $\frac{1}{2}$ UP	2-10-A	1.96×10^6	8.69×10^5	5.71×10^5	5.18×10^5
	2-8-C	1.96×10^6	8.69×10^5	5.71×10^5	2.35×10^5
	1-3-C	4.30×10^6	1.32×10^6	1.18×10^6	4.03×10^5
	1-3-E	4.30×10^6	1.32×10^6	1.18×10^6	1.95×10^6
Unit Train NEC	1-10-C	3.98×10^5	2.53×10^5	1.39×10^5	1.20×10^5
	2-11-A	1.55×10^6	6.70×10^5	4.52×10^5	3.88×10^5
	2-13-A	2.82×10^6	8.84×10^5	8.00×10^5	3.95×10^5
	1-9-A	2.82×10^6	8.84×10^5	8.00×10^5	6.75×10^5
Unit Train SP	1-8-A	3.97×10^7	3.71×10^6	3.55×10^6	$>6.48 \times 10^6$ (b)
	1-9-C	7.67×10^6	1.80×10^6	1.08×10^6	3.84×10^6
	1-4-C	7.74×10^6	1.87×10^6	2.13×10^6	2.01×10^6
Random $\frac{1}{2}$ FEC+ $\frac{1}{2}$ UP	1-6-C	----	----	5.85×10^5	3.78×10^5
	2-1-E	----	----	5.85×10^5	7.13×10^5
	1-13-E	----	----	1.83×10^6	4.11×10^6
	2-6-C	----	----	1.83×10^6	2.09×10^6
Train-by-Train $\frac{1}{2}$ FEC + $\frac{1}{2}$ UP	2-4-C	----	----	1.83×10^6	3.41×10^6
	2-8-A	----	----	3.94×10^6	1.52×10^6

(a) Computed as 94% of actual N_f .

(b) Did not fail.

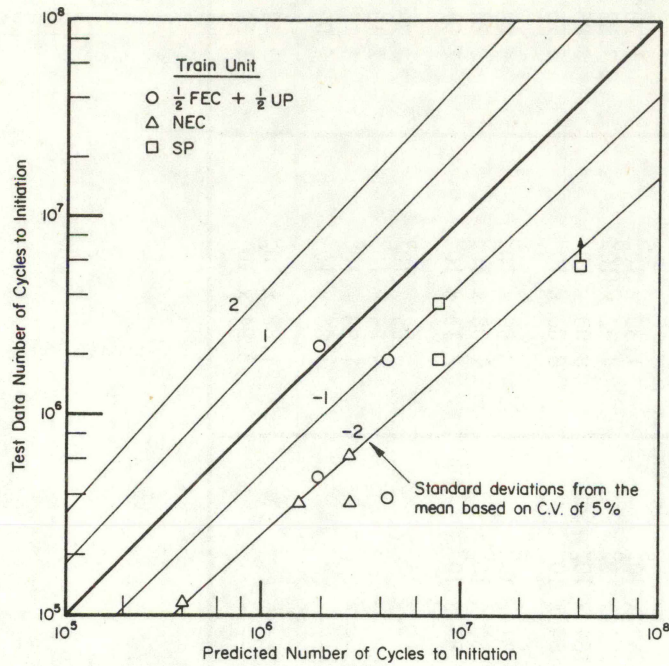


FIGURE 30. METHOD 1, CONSTANT AMPLITUDE CURVE AND ACTUAL MAXIMUM STRESSES (UNIT TRAIN ONLY)

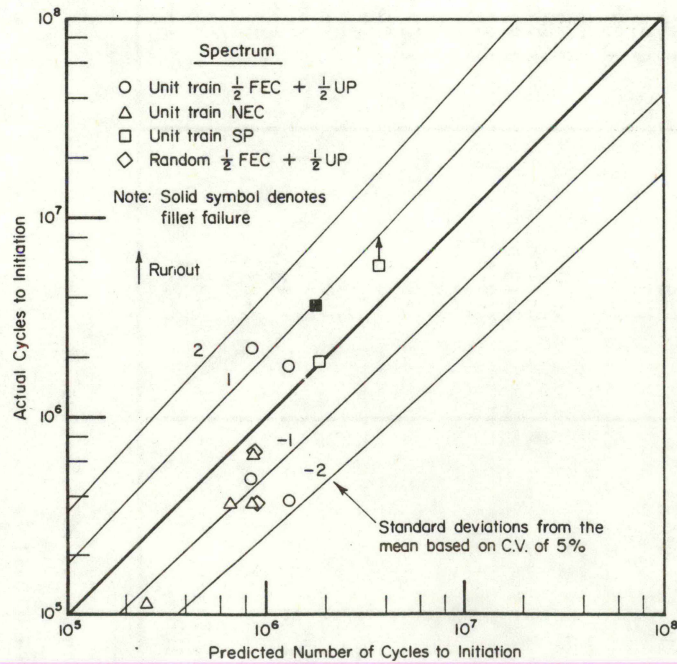


FIGURE 31. METHOD 2, PERIODIC OVERSTRAIN WITH ACTUAL σ_{max}

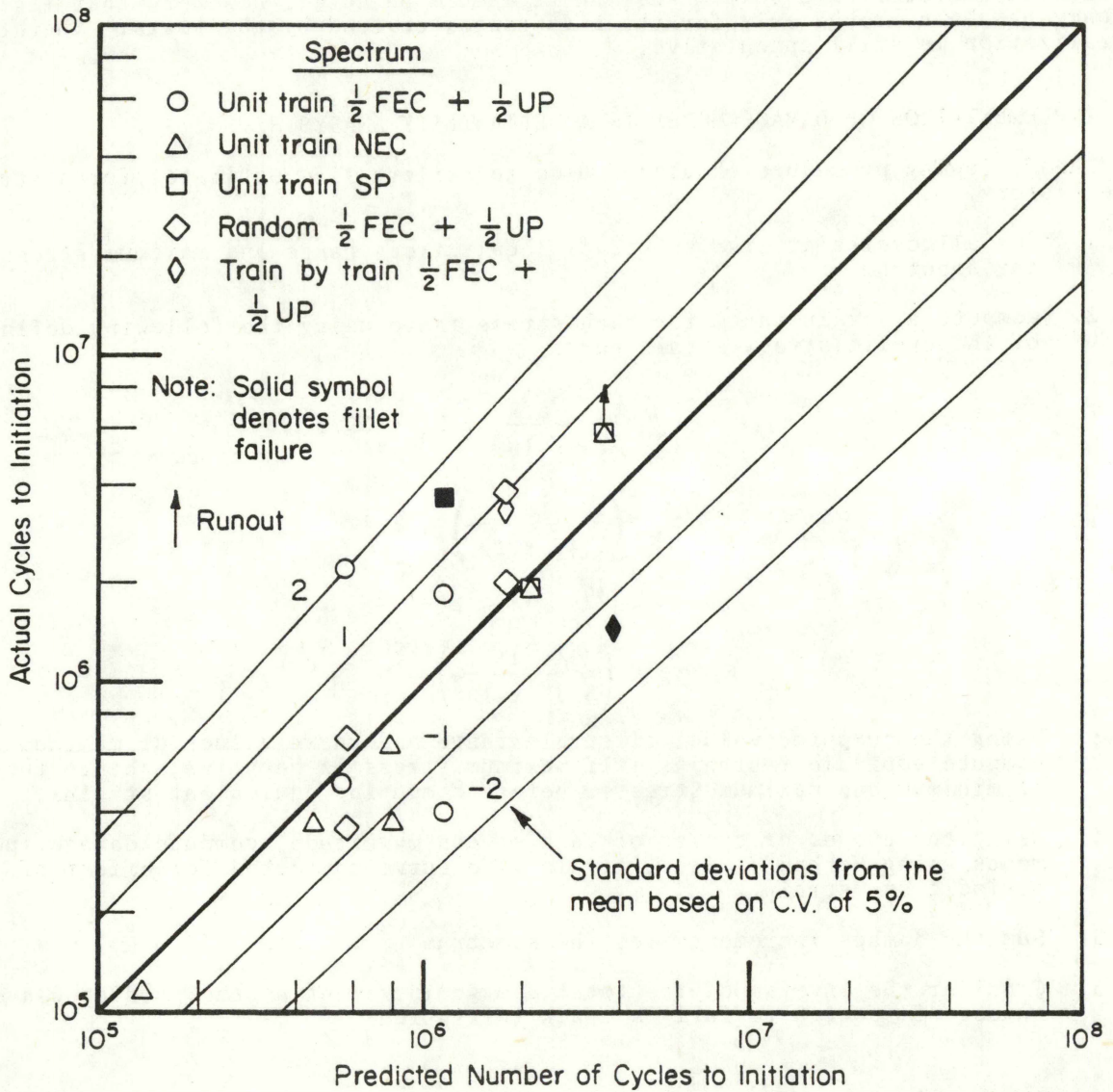


FIGURE 32. METHOD 3, PERIODIC OVERSTRAIN WITH CALCULATED σ_{max}

The predictions based on Method 3 are shown in Figure 32. A similar predictive capability is evident for Method 3, as was shown for Method 2, although it does tend to be somewhat more conservative in the long-life regime. Both Methods 2 and 3 provide predictions nearly as good as the basic scatter in the data.

Neither of the two satisfactory methods included any history or sequence accountability; they represented simple, Miner's rule, linear damage models based on strain-life fatigue curves for test with overstrain cycles. Interestingly, it does not appear that history effects were particularly significant. It is also evident, however, that the second and third damage models were somewhat conservative in the long-life tests which suggests that smaller cycles in these histories may have been non-damaging early in the history, thereby prolonging life in the manner discussed previously for the periodic overstrain data. Lacking a simple and justifiable method for introducing a history dependence in the damage models investigated, it is recommended that the third linear damage method be used in a reliability analysis. The third method is suggested over the second simply because actual stable maximum stresses in a history are seldom known. It should be noted, however, that its adequacy has been proved only for the life ranges covered by the tests. Therefore, generalization is still speculative.

5.4 IMPLEMENTATION OF DAMAGE MODEL IN A RELIABILITY ANALYSIS

The following procedure should be used to perform life estimates for a stress-cycle history.

1. Sum all cycles at like values of local stress range and maximum stress within the spectrum.
2. Compute a strain range for each stress range using the following definition of the cyclic stress-strain curve

$$\epsilon_a = \frac{S_a}{29 \times 10^3}, \quad S_a \leq 39.1$$

$$\epsilon_a = \left(\frac{S_a}{3.43 \times 10^3} \right)^{1.48}, \quad 39.1 < S_a \leq 51.3$$

$$\epsilon_a = \left(\frac{S_a}{8.05 \times 10^2} \right)^{2.26}, \quad S_a > 51.3$$

3. Using the computed values of strain range and known values of maximum stress, compute equivalent strains. If maximum stress is negative, change the sign of minimum and maximum stresses before computing equivalent strains.
4. Using the number of cycles of each stress magnitude, compute damage increments using Method 3, i.e., strain-life curve corrected for effect of periodic overstrain.
5. Sum the damage increments for the spectrum.
6. Consider the inverse of the total damage increment as the predicted average number of spectra to fatigue crack initiation.

6. CONCLUSIONS

From this experimental and analytical investigation of the crack initiation behavior of rail steels, the following conclusions have been made:

1. Periodic overstrains above the constant amplitude endurance limit will substantially increase the damage caused by strain ranges below that limit, and a periodic overstrain fatigue curve should be used in life predictions on such spectra.
2. Transverse rail head crack initiation properties can be expected to fall well below longitudinal rail head properties.
3. Linear damage accumulation models can be expected to provide reasonable life predictions, although such life estimates may become conservative in the very long life histories.
4. There is no definitive transition flaw size, but a flaw of 0.030-inch may serve as a useful transition flaw between crack initiation and propagation.

7. REFERENCES

1. Broek, D., and Rice, R.C., "Fatigue Crack Growth Properties of Rail Steels," Final Report. Part I. FRA/ORD-81/30. NTIS* PB82-129594. October 1981.
2. Broek, D., and Rice, R.C., "Prediction of Fatigue Crack Growth in Rail Steels," Final Report. Part II. October 1981. FRA/ORD-81/31. NTIS PB82-129602.
3. Feddersen, C.E., Buckheit, R.D., and Broek, D., "Fatigue Crack Propagation in Rail Steels," Interim Report. July 1976. FRA/ORD-77/14/NTIS PB272 062/AS.
4. Buckheit, R.D., and Broek, D., "Microstructural and Fractographic Characterization of Fatigue-Tested Rail Steels," Final Report. Part III. No number assigned: publication pending.
5. Klima, S.J., and Freche, J.C., "Ultrasonic Detection and Measurement of Fatigue Cracks in Notched Specimens," Experimental Mechanics, Vol. 9, pp. 193-202, May 1969.
6. Rice, R.C., et al. "Consolidation of Fatigue and Fatigue-Crack-Propagation Data for Design Use," NASA CR-2586, Contractor Report prepared by BCL for NASA Langley Research Center, October 1975.
7. Walker, K., "The Effect of Stress Ratio During Crack Propagation and Fatigue for 2024-T3 and 7075-T6 Aluminum," Effects of Environment and Complex Load History on Fatigue Life, ASTM STP 462, American Society for Testing and Materials, pp 1-14, 1970.
8. Smith, K.N., et al, "A Stress-Strain Function for the Fatigue of Metals," Journal of Materials, JMLSA, 5 (4), pp. 767-778, December 1970.
9. Leis, B.N., and Laflen, J.H., "Cyclic Inelastic Deformation and Fatigue Resistance of a Rail Steel: Experimental Results and Mathematical Models. Interim Report. October 1981. FRA/ORD-81/29. NTIS PB82-129602.
10. Fowler, G.J., "Fatigue Crack Initiation and Propagation in Pearlitic Rail Steels," PhD Dissertation, University of California, Los Angeles, 1976.
11. Kuguel, R., "A Relation Between Theoretical Stress Concentration Factors and Fatigue Notch Factors Deduced from the Concept of Highly Stressed Volume," Proceedings of the ASTM, 61, pp 732-748, 1961.
12. Miner, M.A., "Cumulative Damage in Fatigue," Journal of Applied Mechanics, 12, p. A-159, 1945.
13. Brose, W.R., Dowling, N.E., and Morrow, J., "Effect of Periodic Large Strain Cycles on the Fatigue Behavior of Steels," SAE Paper 740221, 1974.
14. Morrow, J., "Cyclic Plastic Strain Energy and Fatigue of Metals," in Internal Friction, Damping and Cyclic Plasticity, ASTM STP 378, pp. 45-84, 1965.
15. Landgraf, R.W., "Cumulative Fatigue Damage under Complex Strain Histories," in Cyclic Stress-Strain Behavior-Analysis, Experimentation and Prediction, ASTM STP 519, pp 213-228, 1973.
16. Daoud, O.E.K., Cartwright, D.J., and Carney, M., "Strain Energy Release Rate for a Single-Edge-Crack Circular Bar in Tension," Journal of Strain Analysis, 12, (2), 1978.

* National Technical Information Service
5385 Port Royal Road
Springfield, VA 22161

Fatigue Crack Initiation Properties of Rail

**Fatigue Crack Initiation Properties of Rail
Steels, 1982**

US DOT, FRA, RC Rice, D Broek

ONTECO COPY/PRINT

**PROPERTY OF FRA
RESEARCH & DEVELOPMENT
LIBRARY**